The INO80 remodeler couples premature termination of mRNA synthesis with transcription elongation

Sara Luzzi[1], Ugo Szachnowski[2], Sarah Greener[1], Camille Gautier[2], Kang Hoo Han[3], Jack Darke[1], Rossana Piccinno[4], Anne Lafon[2,4], B. Franklin Pugh[3], Antonin Morillon[2*], and Manolis Papamichos-Chronakis[1,5*]

Affiliations:

[1]Biosciences Institute, Faculty of Medical Sciences, Newcastle University, Newcastle upon Tyne, NE2 4HH, United Kingdom.

[2]ncRNA, Epigenetic, and Genome Fluidity, Institut Curie, PSL Research University, CNRS UMR 3244, Pierre et Marie Curie University, 26 rue d'Ulm, 75248 Paris Cedex 05, France.

[3]Center for Eukaryotic Gene Regulation, Department of Biochemistry and Molecular Biology, The Pennsylvania State University, University Park, PA 16802, USA.

[4]Institut Curie, PSL Research University, CNRS, UMR3664, 26 rue d'Ulm, 75248 Paris, France

[5]Lead Contact

*Correspondence to: antonin.morillon@curie.fr and manolis.papamichos@newcastle.ac.uk

SUMMARY

RNA quality control and timely termination of aberrant transcription are critical for functional gene expression. Here, we report that in *Saccharomyces cerevisiae* premature transcription termination of mRNAs is coordinated with the transcriptional elongation process and regulated by the evolutionarily conserved ATP-dependent chromatin remodeling complex INO80. Loss of INO80 sensitizes cells to the transcriptional elongation stress drug 6-azauracil and leads to enhanced pausing of elongating RNA Polymerase II across the genome. Transcriptional pausing positively correlates with premature termination of mRNA transcription and is pronounced proximally to promoters at sites of enhanced histone H3 binding to DNA. Cells with deficient INO80 complex accumulate short, unproductive mRNA transcripts on chromatin and are defective in transcription termination mediated by the Nrd1-Nab3-Sen1 (NNS) complex. We find that loss of INO80 compromises the interaction of the RNA surveillance factor Nab2 with short promoter-proximal mRNA transcripts. INO80 promotes co-transcriptional recruitment of Nab2 to chromatin by enabling its interaction with the histone variant H2A.Z. Finally, inactivation of the histone deacetylase complex Rpd3S/Rco1 reduces promoter-proximal pausing and enhances productive transcription through an NNS-dependent termination site when INO80 is compromised. Our work suggests that, by regulation of H2A.Z-containing nucleosomes, INO80 orchestrates a mechanism for premature transcription termination, linking RNA quality control to the transcriptional process.

INTRODUCTION

Functional gene expression is determined by the balance between productive and unproductive mRNA synthesis. Eukaryotic mRNAs undergo co-transcriptional RNA surveillance and aberrant, non-functional transcripts are prematurely terminated and subsequently degraded. In eukaryotic cells, most mRNAs undergo quality surveillance while the transcript is still attached to elongating RNA polymerase so that non-functional RNAs are prematurely terminated and subsequently degraded (Porrua and Libri, 2013). In the budding yeast *Saccharomyces cerevisiae* non-poly(A)-dependent transcription termination is mediated by the nuclear RNA surveillance complex Nrd1-Nab3-Sen1 (NNS) (Steinmetz et al., 2001). The NNS complex interacts with both the nascent RNA and the RNA Polymerase II (RNAPII) machinery and cooperates with surveillance and RNA cleavage factors such as Nab2 and Hrp1, the nuclear exosome complex and its cofactor TRAMP complex to facilitate transcription termination, RNA processing and degradation by the 3'exonuclease activity of the exosome (Bresson and Tollervey, 2018; Fasken et al., 2015; Porrua and Libri, 2015; Tudek et al., 2014; Vasiljeva and Buratowski, 2006).

A prominent role of the NNS-dependent nuclear RNA quality control and termination pathway is to restrict pervasive transcription of non-coding RNAs (ncRNAs) that extensively takes place from yeast to humans (Jensen et al., 2013). Interestingly, the NNS-dependent pathway has also been proposed to play a global role on mRNA metabolism. In yeast, the NNS components Nrd1 and Nab3 are recruited at active genes with a preference near their 5' end and bind mRNA transcripts (Bresson et al., 2017; Gonzalez-Aguilera et al., 2011; Mayer et al., 2012; Yu et al., 2004). The RNA surveillance and cleavage factors Nab2 and Hrp1 also bind mRNA gene bodies co-transcriptionally (Gonzalez-Aguilera et al., 2011; Yu et al., 2004) and both of them, as well as the TRAMP subunit Mtr4, have been reported to associate with 5'-proximal mRNA fragments of approximately 150 nucleotides in length arising from the majority of mRNA

promoters (Bresson et al., 2017; Tuck and Tollervey, 2013). These results indicate extensive premature termination across the yeast protein-coding genome, particularly proximally to promoters, and suggest that unproductive transcriptional elongation is a wide-spread and common phenomenon, supporting previous reports (Kim et al., 2010; Pelechano et al., 2010). However, a separate report proposed that only a few mRNA genes are subject to transcriptional attenuation by the NNS complex (Schulz et al., 2013). This suggests the existence of additional, unknown regulatory mechanisms that facilitate removal of unproductive RNAPII from chromatin and promote premature termination during transcriptional elongation.

In mammals, short, promoter-associated polyadenylated RNAs have been identified (Kapranov et al., 2007). Here, premature termination and exosome-dependent degradation of mRNA transcripts for a large class of protein-coding genes has been recently described to coincide with promoter-proximal RNAPII pausing sites (Chiu et al., 2018). Experiments with chemical transcriptional inhibitors indicated high rates of turnover and premature termination of promoter-proximal paused RNAPII (Erickson et al., 2018; Krebs et al., 2017; Steurer et al., 2018), suggesting regulation of gene expression by transcriptional attenuation. Furthermore, several studies in higher organisms have reported that production of short, promoter-proximal transcripts is associated with RNAPII pausing and backtracking, and it has a role in regulation of gene expression (reviewed in (Yu et al., 2018)). Despite the fact that promoter-proximal pausing plays a global regulatory role in metazoan transcription (Chen et al., 2018; Gressel et al., 2017; Shao and Zeitlinger, 2017; Taft et al., 2009), the contribution of premature termination to gene regulation and in sustaining productive transcription of functional mRNAs remains poorly understood.

Eukaryotic transcription is highly regulated by histone post-translational covalent modifications and chromatin remodelling. ATP-dependent chromatin remodelling enzymes shape the chromatin landscape and act at almost all stages of RNA production controlling

transcription activation and silencing, modulation of transcriptional rates, transcription termination and RNA export from the nucleus (Babour et al., 2016; Boeger et al., 2008; Morillon et al., 2003; Smolle et al., 2012; Whitehouse et al., 2007). In mammals, premature termination of mRNA genes and promoter-proximal transcriptional pausing have been associated with nucleosome organization (Chiu et al., 2018). However, the role of chromatin remodelers in co-transcriptional RNA quality control remains elusive.

The multisubunit ATP-dependent chromatin remodelling complex INO80 has a well-established and important role in transcription regulation of protein-coding genes across eukaryotes (Poli et al., 2017). INO80 is enriched at the transcription start sites (TSS) of the majority of active and poised mRNA genes in yeast and mammals (Xue et al., 2017; Yen et al., 2013). The nucleosome remodelling activity of INO80 exchanges the histone variant H2A.Z for H2A in nucleosomes and alters nucleosome positions (Poli et al., 2017). While it is generally proposed that the function of INO80 during transcription is to control transcription initiation, the mechanism through which INO80 regulates transcription is not well characterized. Interestingly, INO80 physically interacts with the elongating RNA Polymerase II machinery (Lafon et al., 2015a; Poli et al., 2016) and binds to mRNAs (Edupuganti et al., 2017; Tsvetanova et al., 2010). This suggests an unknown role for INO80 in the transcriptional process.

Here we investigate the role of INO80 in transcription regulation in *S. cerevisiae*. Using the Native Elongating Transcript sequencing (NET-seq) assay we monitor how the process of transcription is regulated by INO80 at nucleotide resolution. We show that INO80 prevents the accumulation of unproductive nascent mRNAs associated with RNAPII on chromatin and alleviates promoter-proximal transcriptional pausing to promote transcription elongation. Our genomic analysis reveals that promoter-proximal pausing of RNAPII is a widespread phenomenon in budding yeast and it is associated with premature transcription termination. We demonstrate that promoter-proximal pausing is established at DNA contact sites for histone H3

between the +1 and +2 nucleosomes independently of INO80. Mechanistically our study indicates that INO80 regulates transcription termination by modulating the interaction between Nab2 and H2A.Z and promoting recruitment of Nab2 to chromatin. Notably, inactivation of the histone deacetylase complex Rpd3S/Rco1 reduces RNAPII pausing and enables productive transcription in cells compromised for INO80-dependent termination. Our results suggest that INO80 regulates a chromatin-mediated pathway for premature transcription termination that controls gene expression.

RESULTS

Sensitivity to transcription elongation stress and accumulation of elongating RNAPII across the protein coding genome in the absence of INO80.

The physical association of INO80 with elongating RNAPII complex (Lafon et al., 2015a; Poli et al., 2016) prompted us to evaluate whether INO80 plays a role in transcription elongation. Wild type (WT) and strains deleted for *INO80* or the INO80-specific subunits *ARP5* or *ARP8* were subjected to transcription elongation stress by 6-azauracil (6-AU), which induces reduction of intracellular GTP and UTP nucleotide pools (Exinger and Lacroute, 1992). Interestingly, deletion of either *INO80, ARP5* or *ARP8* led to a severe growth defect in the presence of 6-AU (Figure 1A and Figure S1A, B), suggesting that the INO80 complex promotes transcriptional elongation by RNAPII.

To provide evidence for a direct involvement of INO80 in transcription elongation we compared the chromatin enrichment of Ino80 and the largest subunit of RNAPII, Rpb1, inside the gene body. In order to exclude any signal from outside the gene body that could potentially skew our analysis we employed ChIP-exo, which provides near single-nucleotide resolution (Rhee and Pugh, 2011, 2012). ChIP-exo analysis for Rpb1 was conducted and compared to

published Ino80 ChIP-exo data (Yen et al., 2013). When ChIP-exo densities were normalized over the total sequencing reads and averaged over gene length, our genome-wide correlation analysis revealed a significant and strong positive correlation between Ino80 and Rpb1 enrichment across mRNA genes ("TSS to PAS", Figure S1C, r=0.68) as well as in the gene body, between 200bp downstream the Transcription Start Site (TSS) and the Poly(A) site (PAS) ("TSS+200 to PAS", Figure 1B, r=0.63). This indicates that the INO80 complex associates with RNAPII inside the gene body, supporting a direct and genome-wide role for INO80 throughout transcription elongation.

To illuminate the role of INO80 in the transcription elongation process, we conducted Native Elongating Transcript NET-seq analysis in WT and *ino80Δ* cells expressing a FLAG-tag version of Rpb1 (Figure S1D). NET-seq captures nascent RNAs bound to transcriptionally engaged RNAPII and sequences the 3'-end of the purified RNAs, thus providing a detailed map of elongating RNAPII across the genome at nucleotide resolution (Churchman and Weissman, 2011). Although the term "nascent RNAs", has been frequently used in the literature to describe newly synthesized RNAs that are not necessarily associated with RNAPII (Wissink et al., 2019), it is supposed to refer to the RNA associated with the polymerase active centre. We will therefore refer to the transcripts captured by NET-seq as "nascent RNAs".

Following normalization over the total sequencing reads, mRNA NET-seq reads were averaged over gene length and compared between the two strains. Our analysis revealed a significant increase in the density of nascent mRNA transcripts by a mean 2.4-fold in *ino80Δ* compared to WT for the vast majority of genes independently of transcription levels (Figure 1C). To test whether the global increase in NET-seq density observed in mRNA genes in the absence of INO80 reflects a true event or it is an artefact of our normalization method on total reads, we conducted an alternative analysis by normalizing the NET-seq reads over the average NET-seq density of the ribosomal protein (RP) genes, which are not affected by deletion of INO80

(Figure S1E). Our analysis using normalization over the RP genes NET density confirmed the increase in NET-seq density in *ino80Δ* for the majority of mRNA genes (Figure S1F), indicating that accumulation of nascent mRNA transcripts on chromatin in the absence of INO80 is a true event. Non-coding nascent transcripts were also increased in *ino80Δ* by at least 2-fold (Figure S1G), in agreement with previous reports (Alcid and Tsukiyama, 2014). However, changes in the abundance of sense and antisense nascent RNAs across mRNA gene regions in *ino80Δ* did not correlate (Figure S1H, r=0.07), suggesting independent functions for INO80 in mRNA and ncRNA transcription.

Metagene analysis for the NET-seq densities in protein-coding genes showed that loss of INO80 led to an increase in the enrichment of nascent mRNA transcripts throughout the gene body compared to WT (Figure 1D). The increase in NET-seq density inside the gene body observed in *ino80Δ* was significantly higher than in the 200bp region upstream the TSS (Figure 1D), and evident in genes with similar NET-seq density between the two strains at the region upstream the TSS (Figure 1E). This excludes the possibility that increased nascent transcript levels in *ino80Δ* result from incoming extragenic transcription.

We asked whether increased NET-seq density inside mRNA genes in *ino80Δ* could be due to upregulated transcription initiation. To test this possibility, we evaluated the enrichment of RNAPII in WT and *ino80Δ* cells by ChIP. Analysis of RNAPII enrichment at the promoter and the promoter-proximal region immediately downstream the TSS provides information on initiation rates. If loss of INO80 led to increased transcription initiation rates, the RNAPII enrichment at the promoter-proximal region would be expected to be increased relative to TSS and higher than in WT. The *NRD1* and *HPT1* genes are amongst the mRNA genes characterized by increased density of nascent RNAs in the absence of INO80 (Figure 1F and Figure S1I). Analysis of Rpb1 enrichment revealed that loss of INO80 led to an increase in RNAPII occupancy in both *NRD1* and *HPT1* promoters, compared to WT cells (Figure 1G and Figure

S1J). However, RNAPII enrichment at the promoter-proximal region of the *NRD1* and *HPT1* genes was not increased in *ino80Δ* but remained comparable to WT (Figure 1G and Figure S1J). In addition, phosphorylation of serine 5 at the Rpb1 C-terminal domain (CTD) (Ser5-P), a hallmark of transcription initiation (Buratowski, 2009), was similar in WT and *ino80Δ* (Figure S1K). Thus, these results contest the hypotheses that increase in nascent mRNAs in the absence of INO80 is due to enhanced transcription initiation.

The role of INO80 in transcription elongation is associated with premature termination and Rrp6-dependent decay.

A large portion of RNAPII molecules bound at the body of protein-coding genes are destined for premature termination (Bresson and Tollervey, 2018; Kim et al., 2010; Pelechano et al., 2010; Tuck and Tollervey, 2013). We hypothesized that the increase in RNAPII density on the body of the protein-coding genome in the absence of INO80 could signify either defective progression of productive RNAPII (slow-down) or compromised premature termination during transcription elongation (Figure 2A). To distinguish between these two possibilities, we asked whether the role of INO80 in counteracting accumulation of RNAPII on chromatin is associated with productive transcription. The rates of productive transcription elongation for protein-coding genes have been calculated in mRNA molecules/hour (nascent Productive Transcription Rates: nPTR) in a genome-wide study conducted at an isogenic yeast strain background to ours (Pelechano et al., 2010). We therefore calculated the Fold-Change in NET-seq densities between *ino80Δ* and WT for the mRNA gene bodies (FC-NET$^{ino80\Delta/\mathrm{WT}}$) and compared it against the published nPTR for each gene. Our analysis indicated a highly significant inverse correlation between FC-NET$^{ino80\Delta/\mathrm{WT}}$ and nPTR (Figure 2B, r= -0.25). This negative association suggests that productively transcribing RNA Polymerases are not assisted by INO80 to move along the gene body. On the contrary, this anticorrelation is in line with a possible role for

INO80 in promoting premature termination during transcription elongation, which could lead to a concomitant decrease in the transcriptional output. We thus addressed whether there is a link between productive transcription and premature termination. RNA binding data for the two RNA surveillance factors Mtr4 or Nab2 have been reported in an isogenic strain background (Tuck and Tollervey, 2013). To generate a Transcription Instability Index (TII) for each mRNA gene, we corrected the Mtr4 and Nab2 RNA binding data for the respective transcription levels as measured by our NET-seq analysis (Figure 2C top panel, and Figure S2A top panel). The two Transcription Instability Indexes TII^{Nab2} and TII^{Mtr4} indicate the level of premature transcription termination for each protein-coding gene. Interestingly, when either TII^{Nab2} or TII^{Mtr4} were plotted against nascent Productive Transcription Rates (nPTR), our analysis revealed an inverse correlation across the protein-coding genome (r= -0.44 and r= -0.46 respectively) (Figure 2C and Figure S2A). A negative correlation was also observed when the nascent Productive Transcription Rates (nPTR) were compared against the TII^{Nab2} values calculated for the gene body region from TSS+200 to PAS (Figure S2B). These results suggest a regulatory crosstalk between premature termination and transcriptional elongation along mRNA genes. Strikingly, comparison of FC-$NET^{ino80\Delta/WT}$ with either TII^{Nab2} or TII^{Mtr4} revealed a highly significant positive correlation between the effect of INO80 on nascent transcription and frequency of RNA surveillance and premature termination (r= 0.34 and r= 0.35 respectively) (Figure 2D and Figure S2C). A similar significant positive correlation between FC-$NET^{ino80\Delta/WT}$ and TII^{Mtr4} was obtained when the analysis was conducted in the gene body away from the promoter region (TSS+200bp to PAS, r=0.39) (Figure S2D). These results suggest that INO80 and the RNA quality control machinery are associated throughout transcriptional elongation.

To test whether accumulation of elongating RNAPII on chromatin role in the absence of INO80 is linked to unproductive transcriptional events, spike-in total RNA-seq analysis was conducted

in *ARP8*-deleted cells lacking the Rrp6 subunit of the nuclear exosome. Genes with either increased or decreased NET-seq density in *ino80Δ* were clustered separately (Figure 1C, pink and grey dots respectively). Box-plot analysis revealed that genes with enhanced accumulation of nascent transcripts on chromatin in *ino80Δ* were characterized by a significantly increased in their RNA levels in the *rrp6Δ arp8Δ* double mutant compared to *rrp6Δ* (Figure 2E, pink boxes). In contrast, genes with no increase in nascent transcripts in *ino80Δ* showed no increase in their mRNA levels in *rrp6Δ arp8Δ* (Figure 2E, grey boxes). Importantly, the Fold-Change in RNA abundance between *rrp6Δ arp8Δ* and *rrp6Δ* (FC-RNA$^{rrp6\Delta arp8\Delta/rrp6\Delta}$) and FC-NET$^{ino80\Delta/\mathrm{WT}}$ positively correlated (Figure 2F, r= 0.38), indicating that counteracting accumulation of RNAPII inside the gene body and suppression of aberrant mRNAs are two associated functions of the INO80 complex during transcriptional elongation.

Enhanced promoter-proximal pausing of RNAPII in the absence of INO80 is linked to exosome-mediated decay.

While we found that recruitment of INO80 inside the gene body is associated with RNAPII, INO80 is preferentially enriched at the promoter-proximal region of mRNA genes, immediately downstream of the TSS (Yen et al., 2013). Metagene analysis of NET-seq reads aligned to TSS in WT cells indicated that elongating RNAPII accumulates approximately 150nt downstream of TSS on average, in agreement with previously published NET-seq data (Churchman and Weissman, 2011) (Figure 3A and Figure S3A). Interestingly, the increase in sense-specific RNAPII accumulation was significantly greater at the promoter-proximal region than at the rest of the gene body in *ino80Δ* (Figure 3A and Figure S3B, C), independently of transcription levels (Figure S3D).

In large sets of genes in mammalian and *Drosophila* cells increased accumulation of RNAPII at the promoter-proximal region has been associated with transcriptional pausing and a delay

in transcriptional elongation (Jonkers and Lis, 2015; Mayer et al., 2017). To evaluate whether the increase in RNAPII accumulation proximally to promoters in *ino80Δ* is linked to defective elongation, we calculated a Traveling Ratio (TR) for mRNA genes in WT and *ino80Δ* (Figure 3B), by analysing the NET-seq read density in the gene body relative to the promoter-proximal region (Rahl et al., 2010). In the absence of INO80, TR was significantly decreased (Figure 3C) in both highly and lowly expressed mRNA genes (Figure S3E). This indicates that accumulation of RNAPII proximally to promoters in *ino80Δ* compromises transcriptional elongation.

To provide additional evidence that transcriptional pausing is enhanced in the absence of INO80, protein-coding genes were sorted and clustered in quartiles according to the Fold-Change in TR between *ino80Δ* and WT ($FC\text{-}TR^{ino80\Delta/WT}$) (Figure 3D). In clusters 1, 2 and 3, reduced TR correlates with enhanced promoter-proximal pausing (Figure 3D, E). Contrary, no evidence of increased pausing in the absence of INO80 was observed in cluster 4, which contains genes in which TR is not decreased in *ino80Δ* (Figure 3D, E). These results suggest that INO80 counteracts RNAPII pausing to promote transcription elongation.

Recent studies in metazoans have suggested that RNA polymerases paused proximally to promoters are targeted for premature termination, with the released RNA undergoing degradation (Chiu et al., 2018; Krebs et al., 2017). To test whether promoter-proximal pausing in yeast is associated with premature termination, we calculated and compared the TR^{WT} and TII^{Mtr4} for the first 200nt after TSS. Our analysis revealed a significant negative correlation between them (Figure 3F, r= -0.45), suggesting a link between promoter-proximal pausing and premature termination. We therefore reasoned that the RNAPII-associated transcripts accumulating proximally to promoters in *ino80Δ* might represent unproductive RNAs targeted for decay. To test this, we analysed the abundance of promoter-proximal transcripts in cells lacking Arp8 and Rrp6 by RNA-seq. While RNA abundance in the gene bodies (TSS+200 to

PAS) was increased in all four clusters in *rrp6Δ arp8Δ* compared to *rrp6Δ* (Figure S3F), deletion of *ARP8* in the *rrp6Δ* strain led to a specific and significant increase in the density of promoter-proximal transcripts (TSS to TSS+200) in clusters 1, 2 and 3, but not in the INO80-independent cluster 4 (Figure 3G). This suggests that the role of INO80 in counteracting accumulation of paused mRNA transcripts on chromatin is associated with suppression of aberrant RNA expression and premature transcription termination.

Alleviation of transcriptional pausing by INO80 is established at DNA binding sites for histone H3.

We subsequently asked whether INO80 regulates the barrier that instigates RNAPII pausing. Since INO80 is a chromatin remodeler, we first investigated whether nucleosomes are involved in INO80-dependent transcriptional pausing. Our analysis focused on the promoter-proximal regions of mRNA genes, given the high impact of INO80 deletion on promoter-proximal pausing and the well-organized nucleosomal structure of the region. Analysis of published MNase nucleosome maps indicated similar promoter-proximal nucleosome enrichment in the four different TR clusters for RNAPII pausing (Figure S4A). Mapping the 3' ends of the nascent mRNA transcripts with respect to nucleosome positioning showed that the promoter-proximal NET-seq density peaks for both WT and *ino80Δ* are not located inside the nucleosome core particle, but at the linker DNA region between the +1 and +2 nucleosomes (Figure S4B). Linker DNA regions have been proposed to be the strongest sites of crosslinking for nucleosomal histone H3, located on average 80bp away from the dyad axis of the neighbouring nucleosomes (Rhee et al., 2014). Intriguingly, analysis of H3 ChIP-exo data in the four TR Clusters indicated that enhanced binding of H3 to the linker DNA is associated with increased promoter-proximal pausing in the absence of INO80 (Figure 4A). This suggests a potential role for histone H3 in RNAPII pausing.

Comparative metagene analysis of NET-seq and H3 ChIP-exo reads confirmed that the NET-seq peak position is located in close proximity to the H3 peak site at the +1/+2 linker DNA in both WT and *ino80Δ* (Figure 4B). However, the genomic enrichment and positioning of histone H3 were similar between WT and *ino80Δ* (Figure 4B), indicating that INO80 does not regulate binding of histone H3 to DNA.

Our analysis led us to evaluate whether promoter-proximal enrichment of nascent transcripts is related to histone H3 positioning. We identified and clustered protein-coding genes with maximum NET-seq density peak between either TSS+50 and +100bp or TSS+100 and +150bp in two separate groups (Figure 4C and Figure S4C) and we mapped the relative H3 ChIP-exo densities in the two clusters. Metagene analysis in the two gene groups demonstrated that the position of H3 peak enrichment was shifted in accordance with the NET-seq peak position in each group, in both WT and *ino80Δ* (Figure 4C and Figure S4C). This result indicates a spatial correlation between transcriptional pausing and histone H3 binding to DNA. To test whether accumulation of elongating RNAPII at the promoter-proximal region is associated with histone H3 occupancy we analysed the NET-seq density profiles in the gene groups with the highest and lowest H3 enrichment at the +1/+2 linker DNA, as defined by 30th percentile cutoff (Figure 4D and Figure S4D). Strikingly, a sharp increase in the density of nascent transcripts at the +1/+2 linker region was observed in genes with high H3 occupancy in the absence of INO80 (Figure 4E and Figure S4E). These results indicate that nucleosomes are involved in instituting promoter-proximal pausing and suggest that INO80 promotes removal of RNAPII accumulating at the nucleosomal H3 barrier.

Defective NNS-dependent transcription termination in the absence of INO80.

Our results established that the role of INO80 in transcription is associated with RNA surveillance and exosome-mediated decay. Coordination between the Nrd1-Nab3-Sen1

complex (NNS), RNA surveillance factors and exosome-associated factors is critical for efficient transcription termination and attenuation of mRNA genes (Fox et al., 2015; Schmid et al., 2012; Steinmetz et al., 2001; Vasiljeva and Buratowski, 2006; Wagschal et al., 2012). We therefore asked whether the role of INO80 in transcription elongation is functionally linked to NNS-dependent transcription termination. *ARP8* was deleted in the *nrd1-V368G* (designated as *nrd1-5,* Figure S5A) mutant strain, which is deficient in transcription termination (Steinmetz et al., 2001). Whereas the *arp8Δ* strain was partially sensitive to 6-AU and the *nrd1-5* mutation itself conferred no apparent sickness in 6-AU, the *nrd1-5 arp8Δ* double mutant strain exhibited synthetic lethality under the same conditions (Figure 5A). Protein co-immunoprecipitation analysis revealed that the INO80 complex physically interacts with both Nrd1 and the surveillance factor Nab2 *in vivo* (Figure 5B, C), but not with the highly abundant Pgk1 protein or the component of cleavage and polyadenylation factor IA (CF IA) complex Pcf11 (Figure 5B, Figure S5B). This suggests that the physical interaction between INO80 and NNS coordinates their functions to ensure productive transcription and functional gene expression.

The physical and functional association of INO80 with the NNS and the nuclear RNA surveillance machinery led us to explore a possible regulatory role for INO80 in NNS-dependent transcriptional termination. To address this, we employed the well-characterized ACT-CUP reporter system for NNS-dependent termination (Arigo et al., 2006; Steinmetz et al., 2001) (Figure S5C). Briefly, cells were transformed with ACT-CUP plasmids without or with the Transcription Termination Site (TTS) of the snoRNA gene *SNR13* (SNR^{TTS}) inserted prior to the *CUP1* gene, which confers resistance to copper. INO80 is co-enriched with Nrd1 at the endogenous $SNR13^{\mathrm{TTS}}$ region (Figure S5D), making the $ACT\text{-}SNR^{TTS}\text{-}CUP$ reporter a suitable system to test the role of INO80 in NNS-dependent transcription termination. Contrary to WT, *ino80Δ* cells transformed with the $ACT\text{-}SNR^{TTS}\text{-}CUP$ plasmid were able to grow in the presence of copper, suggesting read-through transcription of *CUP1* (Figure 5D). RT-qPCR analysis

using primer pairs that target the regions before and after the *SNR13*^{TTS} insertion site in the reporter plasmids (Figure S5E) showed a significant increase in the relative transcription of *CUP1* in the *ACT-SNR*^{TTS}*-CUP* plasmid in *ino80Δ* and *arp8Δ* mutants by 2.8-fold and 3.5-fold respectively (Figure 5E). Similarly, a 3-fold increase was observed in *nrd1-5* cells, in accordance to previous studies (Steinmetz et al., 2001) (Figure 5E). Inducible degradation of INO80 (Jonsson et al., 2004) also resulted in an acute increase in relative *CUP1* levels from the *ACT-SNR*^{TTS}*-CUP* but not from a control *ACT-CUP* plasmid lacking the transcription termination site (Figure S5F). In addition, deletion of either *INO80* or *ARP8* did not significantly alter gene expression of any of the known transcription termination and RNA surveillance factors (Supplementary Table 2). These results support a direct role for INO80 in transcription termination at the *SNR13*^{TTS} termination site.

To further substantiate a role for INO80 in NNS-dependent termination, we evaluated read-through transcription at the transcription termination sites of endogenous snoRNA genes by conducting spiked-in total RNA-seq analysis in WT and *ino80Δ* cells. Identification and analysis of sense RNA-seq reads encompassing the snoRNA^{TTS} revealed a significant increase in the density of read-through transcripts for the majority of the snoRNA genes in the absence of INO80, but not at the ribosomal protein coding gene *YNL096C* (Figure 5F and G, Figure S5G and Supplementary Table 3). The same analysis in cells deleted for the 5'-3' exoribonuclease Xrn1 showed no defect in termination of snoRNAs, as expected, while deletion of Rrp6 compromised termination only at specific snoRNA genes, in accordance with previous studies (Fox et al., 2015; van Dijk et al., 2011) (Figure 5G and Supplementary Table 3). These results indicate that INO80 promotes NNS-dependent transcription termination.

Recruitment of Nab2 to chromatin and its association with H2A.Z are compromised in the absence of INO80.

To understand how INO80 regulates premature termination of mRNAs, we asked whether INO80 promotes the binding of mRNA transcripts to the RNA surveillance machinery. Our analysis focused on the *NRD1* gene, as this is a known target for promoter-proximal premature termination by the NNS pathway (Fox et al., 2015; Steinmetz et al., 2001). Our RNA-IP analysis for Nab2 demonstrated that loss of INO80 led to a significant reduction in the binding of Nab2 to short, promoter-proximal *NRD1* transcripts compared to binding to the PAS-proximal *NRD1* mRNA (*3'-NRD1*) (Figure 6A). This indicates that the mRNA surveillance pathway is compromised in the absence of INO80.

RNA surveillance factors such as Nab2 are recruited at transcribing genes (Gonzalez-Aguilera et al., 2011) and enable co-transcriptional processing of mRNAs. We therefore evaluated whether the recruitment of the RNA quality control machinery on chromatin depends on INO80. Chromatin immunoprecipitations for Nab2-HA and the largest subunit of RNAPII, Rpb1, were conducted in WT and *ino80Δ* in parallel. The Nab2 enrichment was normalized against Rpb1 enrichment in the same region to correct for any changes in transcription between strains. Absence of INO80 led to a significant reduction in the co-transcriptional binding of Nab2 to the promoter-proximal region of *NRD1*, when compared to WT (Figure 6B and Figure S6A). Co-immunoprecipitation for Nab2-HA confirmed that the physical interaction between Nab2 and Rpb1 was not decreased in the absence of INO80 (Figure S6B), excluding the possibility that loss of INO80 compromises the association of Nab2 with RNAPII. This suggests that recruitment of the RNA surveillance machinery to chromatin by INO80 is a critical step in the premature termination pathway of mRNA transcription.

We next sought to gain insight into how chromatin regulation by INO80 promotes recruitment of Nab2 to chromatin. INO80 preferentially remodels nucleosomes containing the histone variant H2A.Z, controlling the dynamics of H2A.Z enrichment on chromatin (Brahma et al., 2017; Eustermann et al., 2018; Papamichos-Chronakis et al., 2011; Yen et al., 2013). Previous

observations in *D. melanogaster* and *S. pombe* have suggested a role for H2A.Z in RNA quality control and non-poly(A) transcription termination (Muniz et al., 2017; Wagner et al., 2007; Zofall et al., 2009). Analysis of published H2A.Z ChIP-exo data (Yen et al., 2013) at the four TR groups showed that increased RNAPII pausing in *ino80Δ* correlated with significant enrichment of H2A.Z at the promoter-proximal region (Figure 6C, Figure S6C). This suggests a link between H2A.Z and co-transcriptional regulation of mRNA quality control.

To test this hypothesis, we asked whether recruitment of Nab2 to chromatin depends on H2A.Z. Chromatin immunoprecipitation analysis showed a significant co-transcriptional decrease of Nab2 enrichment at the promoter-proximal region of *NRD1* in cells lacking *HTZ1*, the gene encoding for H2A.Z in budding yeast, compared to WT (Figure 6D, Figure S6D). Co-immunoprecipitation assays in the absence of nucleic acids demonstrated that H2A.Z interacts with Nab2, even after non-physiological high-salt wash conditions, but not with Pcf11 (Figure 6E, Figure S6E, F). This prompted us to test whether the interaction between H2A.Z and Nab2 is regulated by INO80. Notably, the binding of Nab2 to H2A.Z was compromised in the absence of INO80 (Figure 6E). These results suggest that regulation of H2A.Z by INO80 promotes the interaction between Nab2 and H2A.Z and recruitment of the RNA surveillance machinery to chromatin.

Deletion of *RCO1* decreases the promoter-proximal barrier and rescues productive transcription in *ino80Δ*.

Finally, we asked how uncoupling of RNA quality control from the transcription process impacts on gene expression. Since our analyses point at a role for histone H3 in the INO80-dependent pathway for transcriptional regulation, we hypothesized that chromatin relaxation would relieve promoter-proximal pausing of transcription. Rco1 is a dedicated component of the Histone Deacetylase complex Rpd3S, which deacetylates histone H3 and H4 N-terminal

tails in the gene body (Keogh et al., 2005) suppressing chromatin relaxation during transcriptional elongation (Carrozza et al., 2005). Analysis of published NET-seq data (Churchman and Weissman, 2011) revealed that deletion of *RCO1* reduced the accumulation of nascent transcripts proximally to promoter while significantly increasing the Traveling Ratio (Figure 3B) in mRNA genes (Figure S7A, B). This indicates that the promoter-proximal barrier for RNAPII is reduced upon histone hyperacetylation and provides further evidence that nucleosomes are involved in the establishment and/or maintenance of promoter-proximal transcriptional pausing.

We therefore asked whether histone hyperacetylation in *rco1Δ* could relieve the transcriptional defects observed when INO80 and NNS functions are compromised. In agreement with our hypothesis, deletion of *RCO1* rescued the sensitivity of both *arp8Δ* and *nrd1-5 arp8Δ* mutants to 6-AU (Figure 7A and Figure S7C). This indicates that the interplay between Rpd3S/Rco1 and the INO80/NNS termination pathway regulates transcription elongation.

To test whether coordination between premature termination and release from pausing is a mechanism promoting productive transcription, we asked whether deletion of *RCO1* would affect the expression of *CUP1* from the *ACT-SNR^{TTS}-CUP* plasmid in cells compromised for INO80. Cells deleted for *RCO1* and transformed with the *ACT-SNR^{TTS}-CUP* plasmid failed to grow on copper plates and showed similar rates of *CUP1* transcription to WT (Figure 7B, C). As expected (Steinmetz et al., 2001) the increased read-through transcription of *CUP1* from the *ACT-SNR^{TTS}-CUP* plasmid in *nrd1-5* correlated with formation of viable colonies in the presence of copper (Figure 7B, C). However, the growth of *nrd1-5* cells transformed with *ACT-SNR^{TTS}-CUP* on copper plates was abolished upon deletion of *ARP8* despite the high read-through transcription rates of *CUP1* detected in the double mutant (Figure 7B, C). This suggests that INO80 counteracts the aberrant transcripts expressed in the absence of Nrd1 to facilitate productive *CUP1* transcription. Notably, deletion of *RCO1* in *nrd1-5 arp8Δ* significantly

increased *CUP1* transcription and suppressed the copper-induced lethality of the *nrd1-5 arp8Δ* double mutant (Figure 7B, C). Rescue of growth on 0.4mM copper plates was also observed when *RCO1* was deleted in either *arp8Δ* or *ino80Δ* cells transformed with *ACT-SNR*^{TTS}*-CUP* (Figure S7D). Thus, disruption of Rpd3S/Rco1 restored productive transcription in cells lacking a functional INO80 complex. These results suggest that tampering with the nucleosome barrier for RNAPII pausing for premature transcription termination leads to uncontrollable gene expression.

DISCUSSION

Here, we elucidate a role of INO80 in transcription. We report that INO80 promotes alleviation of paused RNAPII, defining a novel chromatin-based pathway for co-transcriptional mRNA quality control. We provide evidence that INO80 plays a direct role in facilitating NNS-dependent transcriptional termination. Our data suggest that removal of unproductive, paused RNAPII by INO80 promotes transcriptional elongation. Based on our results we propose that control of premature transcriptional termination by INO80 is a crucial and global mechanism for regulation of eukaryotic gene expression (Figure 7D, model).

Previous studies based on analysis of steady-state RNA levels proposed that INO80 suppresses initiation of pervasive transcription (Alcid and Tsukiyama, 2014; Xue et al., 2017). Based on NET-seq analysis, our work indicates enhanced enrichment of elongating RNAPII in *ino80Δ*, which is associated with increased transcriptional pausing and premature termination and anticorrelates with productive transcription rates (Figures 2 and 3). These results suggest that the RNAPII molecules accumulating on chromatin in the absence of INO80 are not engaged in productive transcription, raising the possibility that INO80 targets and promotes removal of non-productive RNAPII from chromatin. Indeed, several lines of evidence argue for a role for INO80 in termination of RNAPII during transcription elongation: (I) INO80 is co-

transcriptionally recruited to coding genes (Figure 1), (II) loss of INO80 leads to defective NNS-dependent transcriptional termination at a plasmid-bore reporter system and increased read-through transcription at the TTSs of endogenous snoRNA genes (Figure 5), (III) INO80 is recruited at transcription termination sites of snoRNAs and physically associates with the Nrd1 and Nab2 components of the RNA cleavage and termination pathway (Figure 5), and (IV) both recruitment of Nab2 to chromatin and its binding to 5'-proximal mRNA depend on INO80 (Figure 6). These results establish an integral role for INO80 in facilitating nuclear RNA quality control that can well-explain the reported increases in expression of mRNAs and ncRNAs observed upon depletion of INO80 (Alcid and Tsukiyama, 2014; Xue et al., 2017).

How does INO80 promote premature termination? Nab2 associates with the RNA cleavage factor Hrp1 (Dheur et al., 2005) and both factors are involved in mRNA quality control and NNS-dependent termination (Kuehner and Brow, 2008; Roth et al., 2005; Tuck and Tollervey, 2013). We therefore postulate that recruitment of Nab2 to chromatin by INO80 enables co-transcriptional cleavage of the nascent RNA, leading to destabilization of the RNAPII elongation complex and subsequent release of RNAPII from chromatin (Figure 7D). As INO80 interacts with and facilitates release of poly-ubiquitinated Rpb1 from chromatin (Lafon et al., 2015a), an intriguing possibility is that Rpb1 ubiquitination is involved in the process, providing specificity and ensuring selective eviction of unproductive RNAPII molecules.

The ATP-dependent nucleosome remodelling activity of INO80 has been proposed to preferentially target and promote eviction of the histone variant H2A.Z from nucleosomes (Brahma et al., 2017; Eustermann et al., 2018; Papamichos-Chronakis et al., 2011). In agreement with a role for H2A.Z in RNA quality control and non-poly(A) transcription termination (Muniz et al., 2017; Wagner et al., 2007; Zofall et al., 2009), our results suggest that INO80 promotes recruitment of Nab2 to chromatin by regulating its interaction with H2A.Z (Figure 6). This implies that remodelling of H2A.Z-containing nucleosomes by INO80 is

important for premature termination. It is therefore likely that intermediate steps in the H2A.Z exchange reaction by INO80, for example disposing of DNA from the surface of H2A.Z-H2B dimers (Brahma et al., 2017), might be involved in regulation of transcription termination by INO80. How H2A.Z promotes recruitment of the RNA quality control machinery to chromatin is not clear. However, it is tempting to speculate that regulation of premature termination entails posttranslational modifications on H2A.Z, which command its dynamic role in the RNA surveillance and termination pathway.

In agreement with earlier studies, our work provides support to the notion that elongating RNAPII is under constant surveillance by the RNA quality control machinery for elimination of unproductive transcripts (Figure 2). Importantly, our findings expand previous studies by revealing that the promoter-proximal region is a hotspot for premature transcription termination (Figure 3). How is the crosstalk between RNA surveillance and transcription established at the chromatin level? By focusing our analysis on the promoter-proximal region, we found that high rates of premature transcription termination positively correlate with enhanced transcriptional pausing taking place at contact sites of histone H3 with linker DNA (Figure 4). Recent reports suggest that the interaction between H3 and linker DNA is dictated by the H3 N-terminal tail (Rhee et al., 2014). This is intriguing as *in vitro* evidence suggest that the N-terminal tail of H3 obstructs RNAPII progression if unacetylated, (Bintu et al., 2012), whilst it also regulates the remodelling activity of INO80 (Ayala et al., 2018). Indeed, our findings that loss of the HDAC component Rco1 alleviates pausing of RNAPII and increases productive transcription elongation from a compromised NNS-dependent termination site (Figure 7) suggest that coordination between premature termination and elongation is regulated by the acetylation status of histone H3 N-terminal tail. Whether other histone post-translational modifications, such as H3K4 methylation, which has been suggested to promote NNS-dependent termination (Terzi et al., 2011), are also involved in RNA surveillance of protein-coding transcripts remains

to be investigated. However, we should also point out that in our model, while nucleosomes are important for RNAPII stalling, nucleosome sliding or reducing nucleosome occupancy do not appear to be required for INO80-dependent RNAPII removal. In conclusion, our results suggest that by regulating pausing of RNAPII during transcription elongation, chromatin structure establishes an RNA quality control checkpoint that dictates the choice between INO80-dependent premature termination and productive transcription elongation.

Promoter-proximal transcriptional pausing has recently been linked to premature termination in metazoans (Chiu et al., 2018; Erickson et al., 2018; Krebs et al., 2017; Steurer et al., 2018). Uncontrolled transcription elongation and dysregulated RNAPII pausing have been implicated in human disease (Rahl et al., 2010; Zhang et al., 2017b). Mutations in the RNA surveillance machinery have been associated with increased transcriptional stress and genomic instability (Aguilera and Gomez-Gonzalez, 2008), both hallmarks of cancer (Kotsantis et al., 2018). Dysregulated expression of INO80 leads to uncontrolled gene expression and is associated with disease (Poli et al., 2017; Zhang et al., 2017a; Zhou et al., 2016). It is therefore anticipated that our reported chromatin mechanism of co-transcriptional RNA quality control has general relevance for regulation of eukaryotic gene expression and in disease.

References

Aguilera, A., and Gomez-Gonzalez, B. (2008). Genome instability: a mechanistic view of its causes and consequences. Nat Rev Genet *9*, 204-217.
Alcid, E.A., and Tsukiyama, T. (2014). ATP-dependent chromatin remodeling shapes the long noncoding RNA landscape. Genes Dev *28*, 2348-2360.
Arigo, J.T., Carroll, K.L., Ames, J.M., and Corden, J.L. (2006). Regulation of yeast NRD1 expression by premature transcription termination. Mol Cell *21*, 641-651.
Ayala, R., Willhoft, O., Aramayo, R.J., Wilkinson, M., McCormack, E.A., Ocloo, L., Wigley, D.B., and Zhang, X. (2018). Structure and regulation of the human INO80-nucleosome complex. Nature *556*, 391-395.
Babour, A., Shen, Q., Dos-Santos, J., Murray, S., Gay, A., Challal, D., Fasken, M., Palancade, B., Corbett, A., Libri, D*., et al.* (2016). The Chromatin Remodeler ISW1 Is a Quality Control Factor that Surveys Nuclear mRNP Biogenesis. Cell *167*, 1201-1214 e1215.
Bacikova, V., Pasulka, J., Kubicek, K., and Stefl, R. (2014). Structure and semi-sequence-specific RNA binding of Nrd1. Nucleic Acids Res *42*, 8024-8038.
Bintu, L., Ishibashi, T., Dangkulwanich, M., Wu, Y.Y., Lubkowska, L., Kashlev, M., and Bustamante, C. (2012). Nucleosomal elements that control the topography of the barrier to transcription. Cell *151*, 738-749.
Boeger, H., Griesenbeck, J., and Kornberg, R.D. (2008). Nucleosome retention and the stochastic nature of promoter chromatin remodeling for transcription. Cell *133*, 716-726.
Brahma, S., Udugama, M.I., Kim, J., Hada, A., Bhardwaj, S.K., Hailu, S.G., Lee, T.H., and Bartholomew, B. (2017). INO80 exchanges H2A.Z for H2A by translocating on DNA proximal to histone dimers. Nat Commun *8*, 15616.
Bresson, S., and Tollervey, D. (2018). Surveillance-ready transcription: nuclear RNA decay as a default fate. Open Biol *8*.
Bresson, S., Tuck, A., Staneva, D., and Tollervey, D. (2017). Nuclear RNA Decay Pathways Aid Rapid Remodeling of Gene Expression in Yeast. Mol Cell *65*, 787-800 e785.
Buratowski, S. (2009). Progression through the RNA polymerase II CTD cycle. Mol Cell *36*, 541-546.
Carrozza, M.J., Li, B., Florens, L., Suganuma, T., Swanson, S.K., Lee, K.K., Shia, W.J., Anderson, S., Yates, J., Washburn, M.P*., et al.* (2005). Histone H3 methylation by Set2 directs deacetylation of coding regions by Rpd3S to suppress spurious intragenic transcription. Cell *123*, 581-592.
Chen, F.X., Smith, E.R., and Shilatifard, A. (2018). Born to run: control of transcription elongation by RNA polymerase II. Nat Rev Mol Cell Biol.
Chiu, A.C., Suzuki, H.I., Wu, X., Mahat, D.B., Kriz, A.J., and Sharp, P.A. (2018). Transcriptional Pause Sites Delineate Stable Nucleosome-Associated Premature Polyadenylation Suppressed by U1 snRNP. Mol Cell *69*, 648-663 e647.
Churchman, L.S., and Weissman, J.S. (2011). Nascent transcript sequencing visualizes transcription at nucleotide resolution. Nature *469*, 368-373.
Churchman, L.S., and Weissman, J.S. (2012). Native elongating transcript sequencing (NET-seq). Curr Protoc Mol Biol *Chapter 4*, Unit 4 14 11-17.
Creamer, T.J., Darby, M.M., Jamonnak, N., Schaughency, P., Hao, H., Wheelan, S.J., and Corden, J.L. (2011). Transcriptome-wide binding sites for components of the Saccharomyces cerevisiae non-poly(A) termination pathway: Nrd1, Nab3, and Sen1. PLoS Genet *7*, e1002329.

Descrimes, M., Ben Zouari, Y., Wery, M., Legendre, R., Gautheret, D., and Morillon, A. (2015). VING: a software for visualization of deep sequencing signals. BMC Res Notes *8*, 419.
Dheur, S., Nykamp, K.R., Viphakone, N., Swanson, M.S., and Minvielle-Sebastia, L. (2005). Yeast mRNA Poly(A) tail length control can be reconstituted in vitro in the absence of Pab1p-dependent Poly(A) nuclease activity. J Biol Chem *280*, 24532-24538.
Edupuganti, R.R., Geiger, S., Lindeboom, R.G.H., Shi, H., Hsu, P.J., Lu, Z., Wang, S.Y., Baltissen, M.P.A., Jansen, P., Rossa, M.*, et al.* (2017). N(6)-methyladenosine (m(6)A) recruits and repels proteins to regulate mRNA homeostasis. Nat Struct Mol Biol *24*, 870-878.
Erickson, B., Sheridan, R.M., Cortazar, M., and Bentley, D.L. (2018). Dynamic turnover of paused Pol II complexes at human promoters. Genes Dev.
Eustermann, S., Schall, K., Kostrewa, D., Lakomek, K., Strauss, M., Moldt, M., and Hopfner, K.P. (2018). Structural basis for ATP-dependent chromatin remodelling by the INO80 complex. Nature *556*, 386-390.
Exinger, F., and Lacroute, F. (1992). 6-Azauracil inhibition of GTP biosynthesis in Saccharomyces cerevisiae. Curr Genet *22*, 9-11.
Fasken, M.B., Laribee, R.N., and Corbett, A.H. (2015). Nab3 facilitates the function of the TRAMP complex in RNA processing via recruitment of Rrp6 independent of Nrd1. PLoS Genet *11*, e1005044.
Fox, M.J., Gao, H., Smith-Kinnaman, W.R., Liu, Y., and Mosley, A.L. (2015). The exosome component Rrp6 is required for RNA polymerase II termination at specific targets of the Nrd1-Nab3 pathway. PLoS Genet *11*, e1004999.
Gonzalez-Aguilera, C., Tous, C., Babiano, R., de la Cruz, J., Luna, R., and Aguilera, A. (2011). Nab2 functions in the metabolism of RNA driven by polymerases II and III. Mol Biol Cell *22*, 2729-2740.
Gressel, S., Schwalb, B., Decker, T.M., Qin, W., Leonhardt, H., Eick, D., and Cramer, P. (2017). CDK9-dependent RNA polymerase II pausing controls transcription initiation. Elife *6*.
Hemming, S.A., Jansma, D.B., Macgregor, P.F., Goryachev, A., Friesen, J.D., and Edwards, A.M. (2000). RNA polymerase II subunit Rpb9 regulates transcription elongation in vivo. J Biol Chem *275*, 35506-35511.
Jensen, T.H., Jacquier, A., and Libri, D. (2013). Dealing with pervasive transcription. Mol Cell *52*, 473-484.
Jonkers, I., and Lis, J.T. (2015). Getting up to speed with transcription elongation by RNA polymerase II. Nat Rev Mol Cell Biol *16*, 167-177.
Jonsson, Z.O., Jha, S., Wohlschlegel, J.A., and Dutta, A. (2004). Rvb1p/Rvb2p recruit Arp5p and assemble a functional Ino80 chromatin remodeling complex. Mol Cell *16*, 465-477.
Kapranov, P., Cheng, J., Dike, S., Nix, D.A., Duttagupta, R., Willingham, A.T., Stadler, P.F., Hertel, J., Hackermuller, J., Hofacker, I.L.*, et al.* (2007). RNA maps reveal new RNA classes and a possible function for pervasive transcription. Science *316*, 1484-1488.
Keogh, M.C., Kurdistani, S.K., Morris, S.A., Ahn, S.H., Podolny, V., Collins, S.R., Schuldiner, M., Chin, K., Punna, T., Thompson, N.J.*, et al.* (2005). Cotranscriptional set2 methylation of histone H3 lysine 36 recruits a repressive Rpd3 complex. Cell *123*, 593-605.
Kim, T.S., Liu, C.L., Yassour, M., Holik, J., Friedman, N., Buratowski, S., and Rando, O.J. (2010). RNA polymerase mapping during stress responses reveals widespread nonproductive transcription in yeast. Genome Biol *11*, R75.
Kotsantis, P., Petermann, E., and Boulton, S.J. (2018). Mechanisms of Oncogene-Induced Replication Stress: Jigsaw Falling into Place. Cancer Discov *8*, 537-555.

Krebs, A.R., Imanci, D., Hoerner, L., Gaidatzis, D., Burger, L., and Schubeler, D. (2017). Genome-wide Single-Molecule Footprinting Reveals High RNA Polymerase II Turnover at Paused Promoters. Mol Cell *67*, 411-422 e414.
Kuehner, J.N., and Brow, D.A. (2008). Regulation of a eukaryotic gene by GTP-dependent start site selection and transcription attenuation. Mol Cell *31*, 201-211.
Lafon, A., Taranum, S., Pietrocola, F., Dingli, F., Loew, D., Brahma, S., Bartholomew, B., and Papamichos-Chronakis, M. (2015a). INO80 Chromatin Remodeler Facilitates Release of RNA Polymerase II from Chromatin for Ubiquitin-Mediated Proteasomal Degradation. Mol Cell *60*, 784-796.
Lafon, A., Taranum, S., Pietrocola, F., Dingli, F., Loew, D., Brahma, S., Bartholomew, B., and Papamichos-Chronakis, M. (2015b). INO80 Chromatin Remodeler Facilitates Release of RNA Polymerase II from Chromatin for Ubiquitin-Mediated Proteasomal Degradation. Mol Cell *60*, 784-796.
Langmead, B., and Salzberg, S.L. (2012). Fast gapped-read alignment with Bowtie 2. Nat Methods *9*, 357-359.
Langmead, B., Trapnell, C., Pop, M., and Salzberg, S.L. (2009). Ultrafast and memory-efficient alignment of short DNA sequences to the human genome. Genome Biol *10*, R25.
Mayer, A., Heidemann, M., Lidschreiber, M., Schreieck, A., Sun, M., Hintermair, C., Kremmer, E., Eick, D., and Cramer, P. (2012). CTD tyrosine phosphorylation impairs termination factor recruitment to RNA polymerase II. Science *336*, 1723-1725.
Mayer, A., Landry, H.M., and Churchman, L.S. (2017). Pause & go: from the discovery of RNA polymerase pausing to its functional implications. Curr Opin Cell Biol *46*, 72-80.
Morillon, A., Karabetsou, N., O'Sullivan, J., Kent, N., Proudfoot, N., and Mellor, J. (2003). Isw1 chromatin remodeling ATPase coordinates transcription elongation and termination by RNA polymerase II. Cell *115*, 425-435.
Muniz, L., Deb, M.K., Aguirrebengoa, M., Lazorthes, S., Trouche, D., and Nicolas, E. (2017). Control of Gene Expression in Senescence through Transcriptional Read-Through of Convergent Protein-Coding Genes. Cell Rep *21*, 2433-2446.
Nagalakshmi, U., Wang, Z., Waern, K., Shou, C., Raha, D., Gerstein, M., and Snyder, M. (2008). The transcriptional landscape of the yeast genome defined by RNA sequencing. Science *320*, 1344-1349.
Papamichos-Chronakis, M., and Peterson, C.L. (2008). The Ino80 chromatin-remodeling enzyme regulates replisome function and stability. Nat Struct Mol Biol *15*, 338-345.
Papamichos-Chronakis, M., Watanabe, S., Rando, O.J., and Peterson, C.L. (2011). Global regulation of H2A.Z localization by the INO80 chromatin-remodeling enzyme is essential for genome integrity. Cell *144*, 200-213.
Pelechano, V., Chavez, S., and Perez-Ortin, J.E. (2010). A complete set of nascent transcription rates for yeast genes. PLoS One *5*, e15442.
Poli, J., Gasser, S.M., and Papamichos-Chronakis, M. (2017). The INO80 remodeller in transcription, replication and repair. Philos Trans R Soc Lond B Biol Sci *372*.
Poli, J., Gerhold, C.B., Tosi, A., Hustedt, N., Seeber, A., Sack, R., Herzog, F., Pasero, P., Shimada, K., Hopfner, K.P.*, et al.* (2016). Mec1, INO80, and the PAF1 complex cooperate to limit transcription replication conflicts through RNAPII removal during replication stress. Genes Dev *30*, 337-354.
Porrua, O., and Libri, D. (2013). RNA quality control in the nucleus: the Angels' share of RNA. Biochim Biophys Acta *1829*, 604-611.

Porrua, O., and Libri, D. (2015). Transcription termination and the control of the transcriptome: why, where and how to stop. Nat Rev Mol Cell Biol *16*, 190-202.
Rahl, P.B., Lin, C.Y., Seila, A.C., Flynn, R.A., McCuine, S., Burge, C.B., Sharp, P.A., and Young, R.A. (2010). c-Myc regulates transcriptional pause release. Cell *141*, 432-445.
Rhee, H.S., Bataille, A.R., Zhang, L., and Pugh, B.F. (2014). Subnucleosomal structures and nucleosome asymmetry across a genome. Cell *159*, 1377-1388.
Rhee, H.S., and Pugh, B.F. (2011). Comprehensive genome-wide protein-DNA interactions detected at single-nucleotide resolution. Cell *147*, 1408-1419.
Rhee, H.S., and Pugh, B.F. (2012). ChIP-exo method for identifying genomic location of DNA-binding proteins with near-single-nucleotide accuracy. Curr Protoc Mol Biol *Chapter 21*, Unit 21 24.
Riles, L., Shaw, R.J., Johnston, M., and Reines, D. (2004). Large-scale screening of yeast mutants for sensitivity to the IMP dehydrogenase inhibitor 6-azauracil. Yeast *21*, 241-248.
Roth, K.M., Wolf, M.K., Rossi, M., and Butler, J.S. (2005). The nuclear exosome contributes to autogenous control of NAB2 mRNA levels. Mol Cell Biol *25*, 1577-1585.
Sandell, L.L., and Zakian, V.A. (1993). Loss of a yeast telomere: arrest, recovery, and chromosome loss. Cell *75*, 729-739.
Schmid, M., Poulsen, M.B., Olszewski, P., Pelechano, V., Saguez, C., Gupta, I., Steinmetz, L.M., Moore, C., and Jensen, T.H. (2012). Rrp6p controls mRNA poly(A) tail length and its decoration with poly(A) binding proteins. Mol Cell *47*, 267-280.
Schulz, D., Schwalb, B., Kiesel, A., Baejen, C., Torkler, P., Gagneur, J., Soeding, J., and Cramer, P. (2013). Transcriptome surveillance by selective termination of noncoding RNA synthesis. Cell *155*, 1075-1087.
Selth, L.A., Gilbert, C., and Svejstrup, J.Q. (2009). RNA immunoprecipitation to determine RNA-protein associations in vivo. Cold Spring Harb Protoc *2009*, pdb prot5234.
Shao, W., and Zeitlinger, J. (2017). Paused RNA polymerase II inhibits new transcriptional initiation. Nat Genet *49*, 1045-1051.
Smolle, M., Venkatesh, S., Gogol, M.M., Li, H., Zhang, Y., Florens, L., Washburn, M.P., and Workman, J.L. (2012). Chromatin remodelers Isw1 and Chd1 maintain chromatin structure during transcription by preventing histone exchange. Nat Struct Mol Biol *19*, 884-892.
Steinmetz, E.J., and Brow, D.A. (1996). Repression of gene expression by an exogenous sequence element acting in concert with a heterogeneous nuclear ribonucleoprotein-like protein, Nrd1, and the putative helicase Sen1. Mol Cell Biol *16*, 6993-7003.
Steinmetz, E.J., Conrad, N.K., Brow, D.A., and Corden, J.L. (2001). RNA-binding protein Nrd1 directs poly(A)-independent 3'-end formation of RNA polymerase II transcripts. Nature *413*, 327-331.
Steurer, B., Janssens, R.C., Geverts, B., Geijer, M.E., Wienholz, F., Theil, A.F., Chang, J., Dealy, S., Pothof, J., van Cappellen, W.A.*, et al.* (2018). Live-cell analysis of endogenous GFP-RPB1 uncovers rapid turnover of initiating and promoter-paused RNA Polymerase II. Proc Natl Acad Sci U S A *115*, E4368-E4376.
Taft, R.J., Kaplan, C.D., Simons, C., and Mattick, J.S. (2009). Evolution, biogenesis and function of promoter-associated RNAs. Cell Cycle *8*, 2332-2338.
Terzi, N., Churchman, L.S., Vasiljeva, L., Weissman, J., and Buratowski, S. (2011). H3K4 trimethylation by Set1 promotes efficient termination by the Nrd1-Nab3-Sen1 pathway. Mol Cell Biol *31*, 3569-3583.
Tsvetanova, N.G., Klass, D.M., Salzman, J., and Brown, P.O. (2010). Proteome-wide search reveals unexpected RNA-binding proteins in Saccharomyces cerevisiae. PLoS One *5*.

Tuck, A.C., and Tollervey, D. (2013). A transcriptome-wide atlas of RNP composition reveals diverse classes of mRNAs and lncRNAs. Cell *154*, 996-1009.
Tudek, A., Porrua, O., Kabzinski, T., Lidschreiber, M., Kubicek, K., Fortova, A., Lacroute, F., Vanacova, S., Cramer, P., Stefl, R.*, et al.* (2014). Molecular basis for coordinating transcription termination with noncoding RNA degradation. Mol Cell *55*, 467-481.
van Dijk, E.L., Chen, C.L., d'Aubenton-Carafa, Y., Gourvennec, S., Kwapisz, M., Roche, V., Bertrand, C., Silvain, M., Legoix-Ne, P., Loeillet, S.*, et al.* (2011). XUTs are a class of Xrn1-sensitive antisense regulatory non-coding RNA in yeast. Nature *475*, 114-117.
Vasiljeva, L., and Buratowski, S. (2006). Nrd1 interacts with the nuclear exosome for 3' processing of RNA polymerase II transcripts. Mol Cell *21*, 239-248.
Verma, R., Oania, R., Fang, R., Smith, G.T., and Deshaies, R.J. (2011). Cdc48/p97 mediates UV-dependent turnover of RNA Pol II. Mol Cell *41*, 82-92.
Wagner, E.J., Burch, B.D., Godfrey, A.C., Salzler, H.R., Duronio, R.J., and Marzluff, W.F. (2007). A genome-wide RNA interference screen reveals that variant histones are necessary for replication-dependent histone pre-mRNA processing. Mol Cell *28*, 692-699.
Wagschal, A., Rousset, E., Basavarajaiah, P., Contreras, X., Harwig, A., Laurent-Chabalier, S., Nakamura, M., Chen, X., Zhang, K., Meziane, O.*, et al.* (2012). Microprocessor, Setx, Xrn2, and Rrp6 co-operate to induce premature termination of transcription by RNAPII. Cell *150*, 1147-1157.
Wery, M., Gautier, C., Descrimes, M., Yoda, M., Vennin-Rendos, H., Migeot, V., Gautheret, D., Hermand, D., and Morillon, A. (2018). Native elongating transcript sequencing reveals global anti-correlation between sense and antisense nascent transcription in fission yeast. RNA *24*, 196-208.
Whitehouse, I., Rando, O.J., Delrow, J., and Tsukiyama, T. (2007). Chromatin remodelling at promoters suppresses antisense transcription. Nature *450*, 1031-1035.
Wissink, E.M., Vihervaara, A., Tippens, N.D., and Lis, J.T. (2019). Nascent RNA analyses: tracking transcription and its regulation. Nat Rev Genet.
Xue, Y., Pradhan, S.K., Sun, F., Chronis, C., Tran, N., Su, T., Van, C., Vashisht, A., Wohlschlegel, J., Peterson, C.L.*, et al.* (2017). Mot1, Ino80C, and NC2 Function Coordinately to Regulate Pervasive Transcription in Yeast and Mammals. Mol Cell *67*, 594-607 e594.
Yen, K., Vinayachandran, V., Batta, K., Koerber, R.T., and Pugh, B.F. (2012). Genome-wide nucleosome specificity and directionality of chromatin remodelers. Cell *149*, 1461-1473.
Yen, K., Vinayachandran, V., and Pugh, B.F. (2013). SWR-C and INO80 chromatin remodelers recognize nucleosome-free regions near +1 nucleosomes. Cell *154*, 1246-1256.
Yu, D., Ma, X., Zuo, Z., Wang, H., and Meng, Y. (2018). Classification of Transcription Boundary-Associated RNAs (TBARs) in Animals and Plants. Front Genet *9*, 168.
Yu, M.C., Bachand, F., McBride, A.E., Komili, S., Casolari, J.M., and Silver, P.A. (2004). Arginine methyltransferase affects interactions and recruitment of mRNA processing and export factors. Genes Dev *18*, 2024-2035.
Zhang, S., Zhou, B., Wang, L., Li, P., Bennett, B.D., Snyder, R., Garantziotis, S., Fargo, D.C., Cox, A.D., Chen, L.*, et al.* (2017a). INO80 is required for oncogenic transcription and tumor growth in non-small cell lung cancer. Oncogene *36*, 1430-1439.
Zhang, X., Chiang, H.C., Wang, Y., Zhang, C., Smith, S., Zhao, X., Nair, S.J., Michalek, J., Jatoi, I., Lautner, M.*, et al.* (2017b). Attenuation of RNA polymerase II pausing mitigates BRCA1-associated R-loop accumulation and tumorigenesis. Nat Commun *8*, 15908.

Zhou, B., Wang, L., Zhang, S., Bennett, B.D., He, F., Zhang, Y., Xiong, C., Han, L., Diao, L., Li, P.*, et al.* (2016). INO80 governs superenhancer-mediated oncogenic transcription and tumor growth in melanoma. Genes Dev *30*, 1440-1453.
Zofall, M., Fischer, T., Zhang, K., Zhou, M., Cui, B., Veenstra, T.D., and Grewal, S.I. (2009). Histone H2A.Z cooperates with RNAi and heterochromatin factors to suppress antisense RNAs. Nature *461*, 419-422.

ACKNOWLEDGMENTS

We thank S. Baulande and P. Legoix-Né (NGS platform, Institute Curie). We also thank Maxime Wéry and Nicolas Vogt for outstanding help with the NET-seq and RNA-seq assays and critical reading of the manuscript, David A. Brow for the generous gift of the pGAC24 and pGAC24-SNR13TTS plasmids and the *nrd1-5* yeast strain, and Kuangyu Yen, Lisa Prendergast and members of the Papamichos-Chronakis and Morillon's labs for constructive discussions. This work has benefited from the facilities and expertise of the NGS platform of Institute Curie, supported by the Agence Nationale de la Recherche (ANR-10-EQPX-03, ANR10-INBS-09-08) and the Canceropôle Ile-de-France. MPC is supported by Newcastle University. AM is supported by the Agence Nationale de la Recherche (DNA-Life) and the European Research Council (EPIncRNA starting grant, DARK consolidator grant). This work has received support by the U.S. National Institutes of Health HG004160 to BFP. BFP has a financial interest in Peconic, LLC, which utilizes the ChIP-exo technology implemented in this study and could potentially benefit from the outcomes of this research. Authors declare no competing interests.

Data and materials availability:

Accession numbers: Raw sequences have been deposited to the NCBI Gene Expression Omnibus (accession numbers GSE108046, GSE108053, GSE108054).

Genome browsers for visualization of NET-Seq, RNA-seq and H3 ChIP-exo processed data are accessible at http://vm-gb.curie.fr/Manolis/NET_SEQ_INO80/, http://vm-gb.curie.fr/Manolis/INO_A650/ and http://vm-gb.curie.fr/Manolis/Chipexo/H3 respectively.

All data is available in the main text or the supplementary materials.

FIGURES

Figure 1

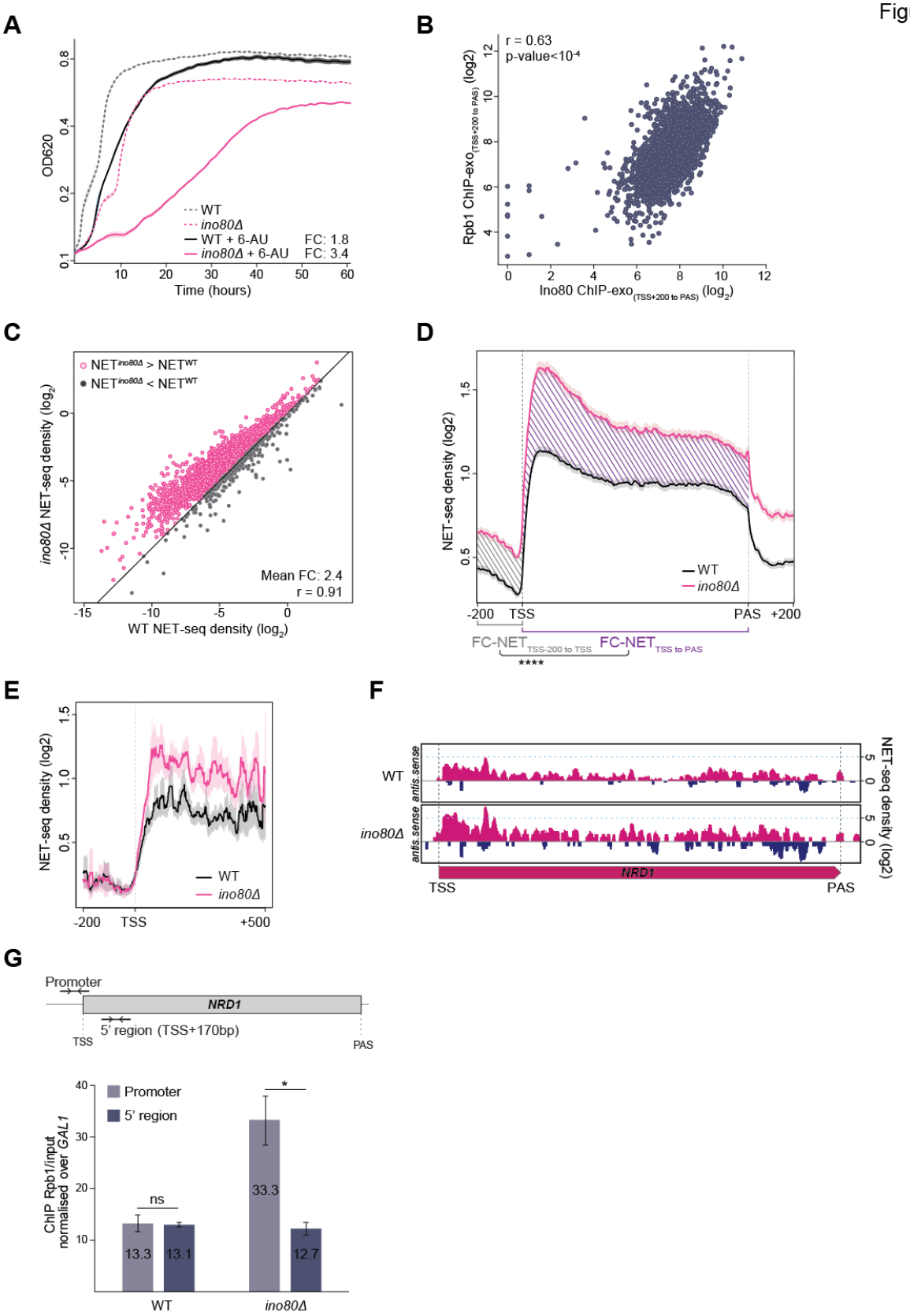

Figure 1. Defective transcriptional elongation and enhanced accumulation of elongating RNAPII along the gene bodies in the absence of INO80.

(A) Cell proliferation analysis for WT and *ino80Δ* strains grown exponentially in SC-ura and in SC-ura containing 50 µg/ml 6-azauracil (6-AU) liquid media for the indicated time. Cell density was measured at OD^{620} and plotted on a log_2 scale. Shading surrounding each line denotes standard error from four independent experiments. Doubling time was calculated from OD^{620}: 0.2 to OD^{620}: 0.4 for all strains in both conditions. Fold Change ratio (FC) of doubling time in 6-AU over SC-ura for each strain is shown.

(B) Scatterplot analysis comparing Ino80 (Yen et al., 2013) and Rpb1 ChIP-exo densities between 200bp downstream of transcription start site (TSS+200bp) and the polyadenylation site (PAS) of the bodies of 5798 mRNA genes. Pearson's correlation coefficient (r) and p-values are indicated.

Scatterplot analysis comparing Ino80 (Yen et al., 2013) and Rpb1 ChIP-exo densities across 5435 mRNA yeast genes. Pearson's correlation coefficient (r) and p-value are indicated.

(C) Scatterplot analysis comparing NET-seq densities in WT and *ino80Δ* for mRNA genes, plotted on a log_2 scale. Pink and grey dots represent genes whose NET-seq density is either higher (5118 genes), or equal or lower (317 genes), respectively, in *ino80Δ* compared to WT. Pearson's correlation coefficient (r) and *ino80Δ*/WT mean Fold-Change (FC) are indicated.

(D) Metagene analysis for NET-seq density profiles averaged across mRNA genes in WT and *ino80Δ*. Tags were aligned to both Transcription Start Site (TSS) and Polyadenylation Site (PAS) for each gene and plotted on a log_2 scale. The shading surrounding each line denotes the 95% confidence interval. The significant difference between changes in nascent transcript density in *ino80Δ* compared to WT over gene regions (purple area, $FC\text{-}NET^{TSS\ to\ PAS}$) and over the 200bp region upstream of TSS (grey area, $FC\text{-}NET^{TSS\text{-}200\ to\ TSS}$) is indicated. p-value was calculated by Wilcoxon rank-sum test. ****, $p < 0.0001$.

(E) Metagene analysis of NET-seq density profiles averaged across 702 mRNA genes with similar density for the 200nt region before TSS in WT and *ino80Δ*. Tags were aligned relative to TSS and plotted on $\log_2$ scale.

(F) NET-seq density profiles in WT and *ino80Δ* for sense and antisense transcripts across the *NRD1* mRNA gene region plotted with VING software (Descrimes et al., 2015).

(G) Chromatin immunoprecipitation for Rpb1 in WT and *ino80Δ* cells. Rpb1 enrichment was measured at either the promoter (Promoter) or the promoter-proximal region (5' region) of the *NRD1* mRNA gene and normalised to the *GAL1* promoter, after correction for input DNA levels. Bars, standard errors from three independent experiments. p-values were calculated by t-test after testing for normal distribution by Shapiro-Wilk test. *, $p<0.05$. ns, not-significant.

See also Figure S1.

Figure 2

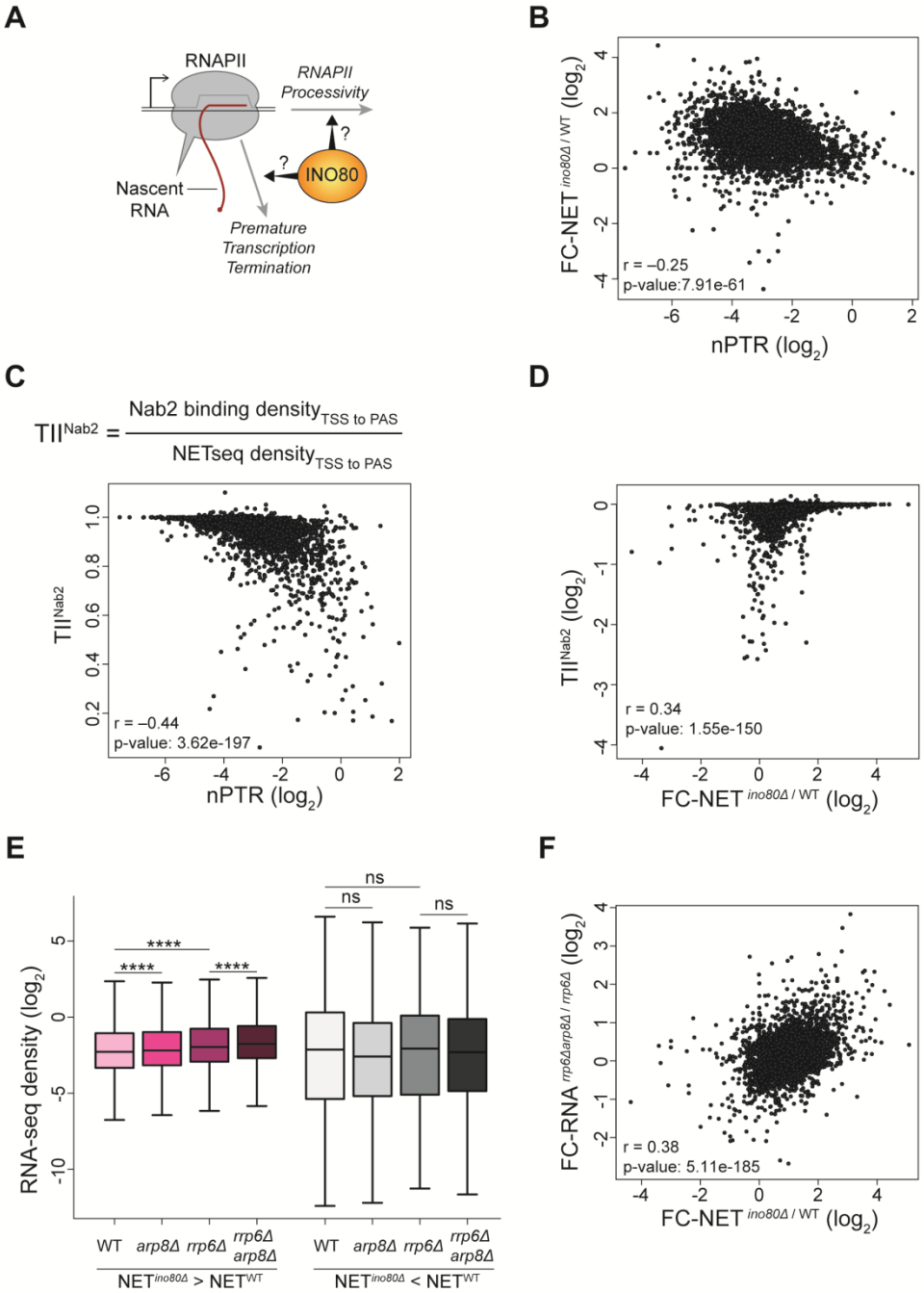
A
RNAPII
RNAPII Processivity
INO80
Nascent RNA
Premature Transcription Termination
B
FC-NET ino80Δ / WT (log2)
nPTR (log2)
r = –0.25
p-value:7.91e-61
C
TII^Nab2 = Nab2 binding density TSS to PAS / NETseq density TSS to PAS
TII^Nab2
nPTR (log2)
r = –0.44
p-value: 3.62e-197
D
TII^Nab2 (log2)
FC-NET ino80Δ / WT (log2)
r = 0.34
p-value: 1.55e-150
E
RNA-seq density (log2)
****
ns
WT
arp8Δ
rrp6Δ
rrp6Δ arp8Δ
NET^ino80Δ > NET^WT
NET^ino80Δ < NET^WT
F
FC-RNA rrp6Δarp8Δ / rrp6Δ (log2)
FC-NET ino80Δ / WT (log2)
r = 0.38
p-value: 5.11e-185

Figure 2. INO80 is associated with premature termination and Rrp6-dependent decay.

(A) Schematic cartoon to explain the increase in nascent transcript density in *ino80Δ*. The function of INO80 either promotes RNAPII processivity during transcription elongation, or it facilitates premature transcription termination.

(B) Scatterplot analysis comparing the *ino80Δ*/WT NET-seq density Fold-Change (FC-NET$^{ino80\Delta/WT}$) and nascent Productive Transcriptional Rates (nPTR) from (Pelechano et al., 2010), both plotted on a $\log_2$ scale. Pearson's correlation coefficient (r) and p-value are indicated.

(C) Upper panel, formula for calculating the Nab2 Transcription Instability Index (TII^{Nab2}) from Nab2 CRAC (Tuck and Tollervey, 2013) and NET-seq densities over mRNA genes in WT (TSS to PAS). Bottom panel, scatter plot analysis comparing TII^{Nab2} and nPTR (Pelechano et al., 2010) over mRNA genes (TSS to PAS). Pearson's correlation coefficient (r) and p-value are indicated.

(D) Scatterplot analysis comparing TII^{Nab2} and the *ino80Δ*/WT NET-seq density Fold-Change (FC-NET$^{ino80\Delta/WT}$), shown on a $\log_2$ scale. Pearson's correlation coefficient (r) and p-value are indicated.

(E) Boxplot analysis comparing RNA-seq densities from the indicated strains. 5435 mRNA genes were clustered in two groups according to the relative increase (left group, NET$^{ino80\Delta}$ > NET^{WT}) or decrease (right group, NET$^{ino80\Delta}$ < NET^{WT}) of NET-seq density in *ino80Δ* compared to WT. p-values were calculated by Wilcoxon rank-sum test. ****, $p<10^{-4}$. ns, non-significant.

(F) Scatterplot analysis comparing the *rrp6Δarp8Δ*/*rrp6Δ* RNA-seq density Fold Change (FC-RNA$^{rrp6\Delta arp8\Delta/rrp6\Delta}$) and the *ino80Δ*/WT NET-seq density Fold-Change (FC-NET$^{ino80\Delta/WT}$), shown on a $\log_2$ scale. Pearson's correlation coefficient (r) and p-value are indicated.

See also Figure S2.

Figure 3

A

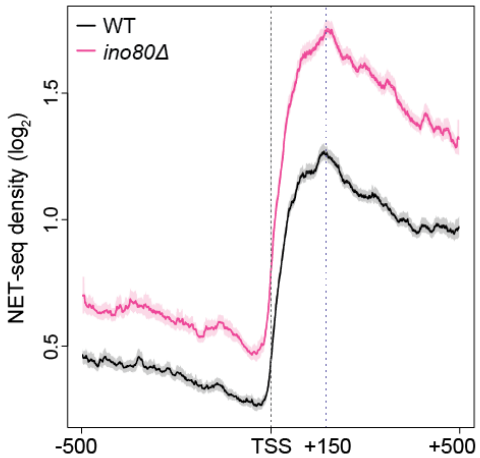

B

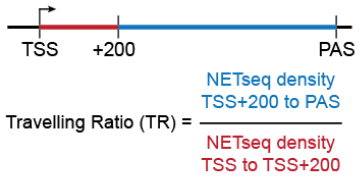

C

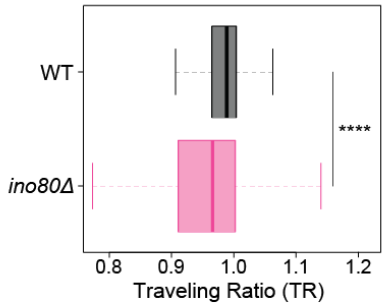

D

	FC-TR $^{ino80\Delta / WT}$	Nr of genes	Pausing in *ino80Δ*
Cluster 1	Highest	1359	Highest
Cluster 2	Mid-high	1359	Mid-high
Cluster 3	Mid-low	1359	Low
Cluster 4	Lowest	1358	No pausing

E

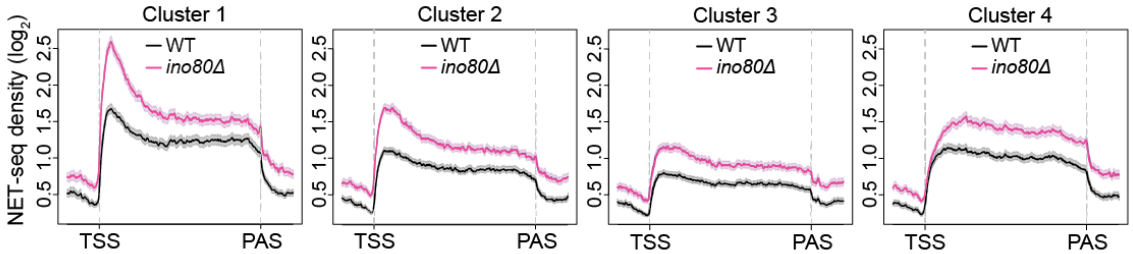

F

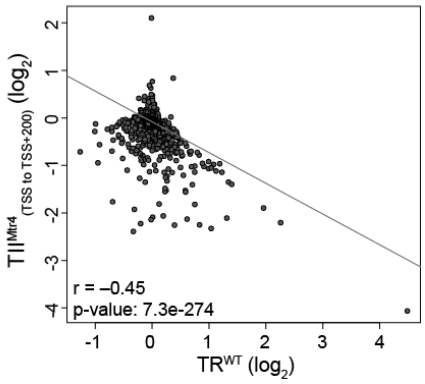

G

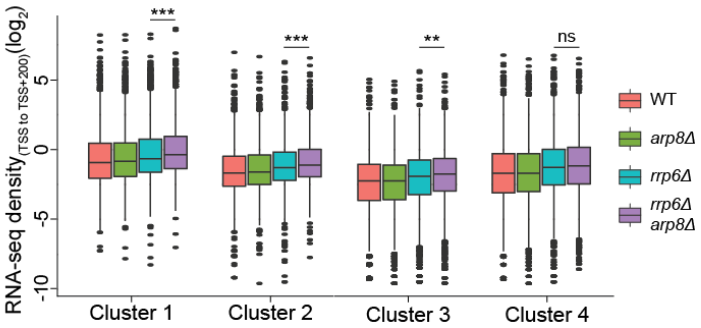

Figure 3. INO80 regulation of promoter-proximal paused RNAPII is associated with exosome-mediated RNA decay.

(A) Metagene analysis for NET-seq density profiles averaged across mRNA genes in WT and *ino80Δ*. Tags were aligned to TSS and plotted on a $\log_2$ scale. The shading surrounding each line denotes the 95% confidence interval. Blue line marks the +150bp location relative to TSS.

(B) Schematic representation and formula for calculating the Traveling Ratio (TR) from NET-seq mRNA densities.

(C) Boxplot analysis of Traveling Ratio for mRNA genes in WT and *ino80Δ*. p-value < 2.2e-16 (****) as calculated by Wilcoxon rank-sum test.

(D) Schematic table for clustering mRNA genes according to the relative TR Fold-Change in *ino80Δ* compared to WT ($\text{FC-TR}^{ino80\Delta/\text{WT}}$). The number of genes and the level of promoter-proximal pausing in *ino80Δ*, as observed by metagene analysis (F), are indicated for each cluster.

(E) Metagene analysis for NET-seq density profiles averaged across mRNA genes in the four gene clusters defined by their relative $\text{FC-TR}^{ino80\Delta/\text{WT}}$, in WT and *ino80Δ*. Tags were aligned to both TSS and PAS and plotted on a $\log_2$ scale. The shading surrounding each line denotes the 95% confidence interval.

(F) Scatterplot analysis comparing Travelling Ratio in WT (TR^{WT}) and Mtr4 Transcription Instability Index (TII^{Mtr4}), calculated from Mtr4 CRAC (Tuck and Tollervey, 2013) and NET-seq densities across the first 200nt region after TSS of mRNA genes (TSS to TSS+200). Pearson's correlation coefficient (r) and p-values are indicated.

(G) Boxplot analysis comparing RNA-seq densities from the indicated strains across the promoter-proximal regions of mRNA genes (TSS to TSS+200bp) in the four clusters defined by their relative $\text{FC-TR}^{ino80\Delta/\text{WT}}$. p-values were calculated by Wilcoxon rank-sum test. ***, p<0.001. **, p<0.01. ns, non-significant.

See also Figure S3.

Figure 4

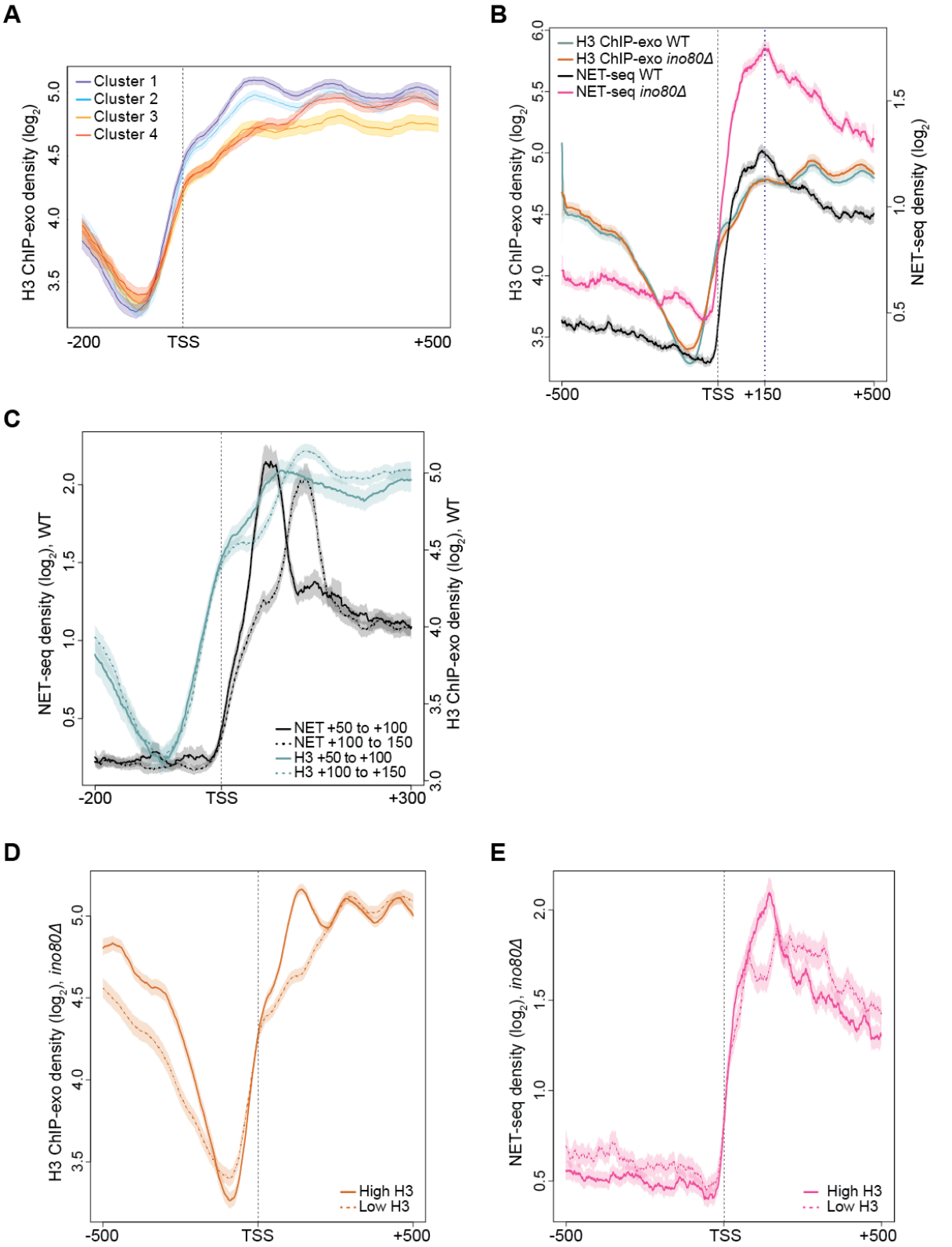
A
Cluster 1
Cluster 2
Cluster 3
Cluster 4
H3 ChIP-exo density (log2)
-200
TSS
+500
B
H3 ChIP-exo WT
H3 ChIP-exo ino80Δ
NET-seq WT
NET-seq ino80Δ
H3 ChIP-exo density (log2)
NET-seq density (log2)
-500
TSS
+150
+500
C
NET-seq density (log2), WT
H3 ChIP-exo density (log2), WT
NET +50 to +100
NET +100 to 150
H3 +50 to +100
H3 +100 to +150
-200
TSS
+300
D
H3 ChIP-exo density (log2), ino80Δ
High H3
Low H3
-500
TSS
+500
E
NET-seq density (log2), ino80Δ
High H3
Low H3
-500
TSS
+500

Figure 4. Promoter-proximal nascent transcripts are retained at histone H3-DNA contact sites in *ino80Δ*.

(A) Metagene analyses for histone H3 ChIP-exo density profiles in WT in the four gene clusters defined by their relative FC-TR$^{ino80\Delta/\mathrm{WT}}$ (Figure 3C). Tags were aligned relative to TSS and plotted on a $\log_2$ scale.

(B) Metagene analysis for NET-seq and histone H3 ChIP-exo density profiles averaged across all mRNA genes in WT and *ino80Δ*. Blue dotted line marks the TSS+150bp site. Data plotted on a $\log_2$ scale.

(C) Metagene analysis for NET-seq and histone H3 ChIP-exo density profiles in WT for mRNA gene clusters with maximum peak of NET-seq density either between +50 and +100bp (solid lines, 501 genes), or between +100 and +150bp (broken lines, 501 genes) from TSS. Data plotted on a $\log_2$ scale.

(D) Metagene analysis for ChIP-exo density profiles for histone H3 in *ino80Δ* for the mRNA genes with highest (solid line) and lowest (broken line) H3 enrichment in the +1/+2 linker using 30th percentile cutoff. Gene lists derived from (Rhee et al., 2014). Data plotted on a $\log_2$ scale.

(E) Metagene analysis for NET-seq density profiles in *ino80Δ* for mRNA genes with highest (solid line) and lowest (broken line) H3 enrichment in the +1/+2 linker using 30th percentile cutoff described in (D). Data plotted on a $\log_2$ scale.

See also Figure S4.

Figure 5

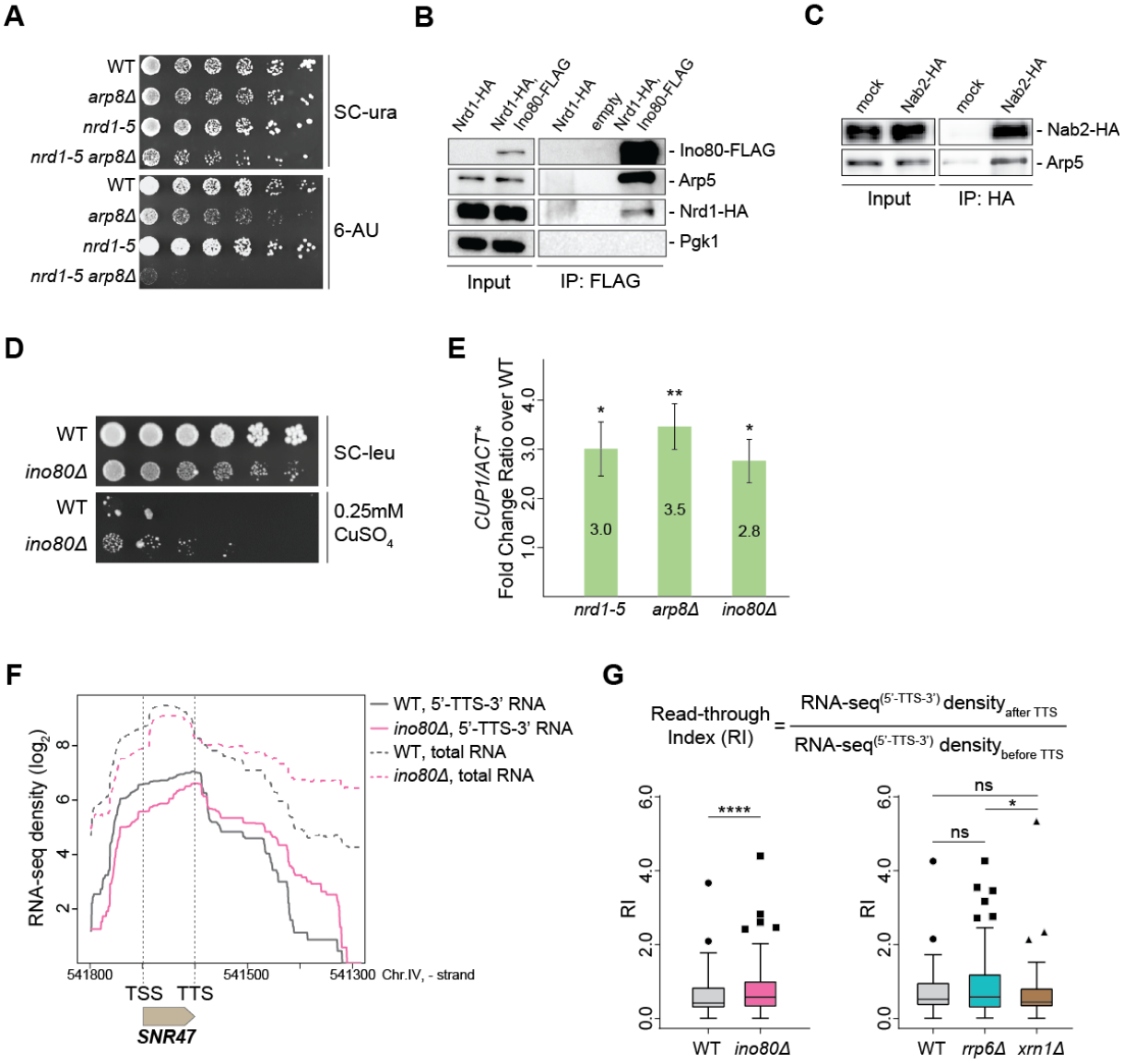
A
WT
arp8Δ
nrd1-5
nrd1-5 arp8Δ
SC-ura
6-AU
B
Nrd1-HA
Nrd1-HA, Ino80-FLAG
Nrd1-HA
empty
Nrd1-HA, Ino80-FLAG
- Ino80-FLAG
- Arp5
- Nrd1-HA
- Pgk1
Input
IP: FLAG
C
mock
Nab2-HA
mock
Nab2-HA
- Nab2-HA
- Arp5
Input
IP: HA
D
WT
ino80Δ
SC-leu
0.25mM CuSO4
E
CUP1/ACT* Fold Change Ratio over WT
3.0
3.5
2.8
nrd1-5
arp8Δ
ino80Δ
F
RNA-seq density (log2)
WT, 5'-TTS-3' RNA
ino80Δ, 5'-TTS-3' RNA
WT, total RNA
ino80Δ, total RNA
541800
541500
541300 Chr.IV, - strand
TSS
TTS
SNR47
G
Read-through Index (RI) = RNA-seq(5'-TTS-3') density after TTS / RNA-seq(5'-TTS-3') density before TTS
RI
****
ns
*
WT
ino80Δ
rrp6Δ
xrn1Δ

Figure 5. Defective NNS-dependent transcriptional termination in *ino80Δ*.

(A) 5-fold serial dilution of cells from the indicated strains were plated onto both SC-ura and SC-ura + 50µg/ml 6-Azauracil (6-AU) and incubated at 30ºC for 4-5 days.

(B) Nucleic acid-free lysates from cells co-expressing Nrd1-HA with Ino80 either untagged or tagged with FLAG epitope were subjected to FLAG-IP. Inputs and IP samples were immunoblotted for FLAG, Arp5, HA. Immunoblot against Pgk1 served as a control.

(C) Nucleic acid-free lysates from cells expressing Nab2-HA were subjected to either HA-IP (Nab2-HA) or IgG-IP (mock). Inputs and IP samples were immunoblotted for Arp5 and HA.

(D) 5-fold serial dilution of cells from the indicated strains were plated onto both SC-leu and SC-leu + 0.25mM $CuSO_4$ and incubated at 30ºC for 3 (SC-leu) and 7 days ($CuSO_4$).

(E) RT-qPCR analysis was conducted in WT, *nrd1-5*, *arp8Δ* and *ino80Δ* cells transformed with either *ACT-CUP* or *ACT-SNR^{TTS}-CUP* plasmids. The *CUP1/ACT** ratio from the *ACT-SNR^{TTS}-CUP* plasmid was normalized over the same ratio from the control *ACT-CUP* plasmid (Figure S4E) to correct for differential transcription across all strains. Read-through at the *SNR13^{TTS}* for each indicated strain is shown as Fold Change Ratio over WT. Bars, standard errors from three independent experiments. p-values were calculated by t-test after testing for normal distribution by Shapiro-Wilk test. *, $p<0.05$. **, $p<0.01$.

(F) Snapshot of RNA-seq densities in WT and *ino80Δ* across the *SNR47* snoRNA gene. Solid lines, density of reads encompassing the transcription termination site (5'-TTS-3') of the *SNR47* gene. Broken lines, total RNA-seq density. Reads encompassing the TTS were selected from the total RNA-seq reads as containing 5' upstream the *SNR47* TTS and 3' at or after the *SNR47* TTS. Genomic coordinates of Chromosome IV around the *SNR47* gene (coordinates: 541700 to 541602) are shown. The closest downstream gene is *YDR042C* (TSS: Chromosome IV, 541203).

(G) Upper panel, formula for calculating the Read-through Index (RI) from RNA-seq densities across snoRNA genes that encompass transcription termination sites (TTS). RNA-seq reads with 5' upstream the TTS and 3' at or after the TTS were selected from the total RNA-seq read pool and the ratio of the RNA-seq read density after TTS to the RNA-seq read density before TTS in the selected reads was calculated. Lower panel, boxplot analysis comparing RI from the indicated strains across snoRNA genes. p-values were calculated by Wilcoxon matched-pairs rank test after testing for normal distribution. ****, $p<0.0001$. *, $p<0.05$. ns, non-significant. *See also Figure S5.*

Figure 6

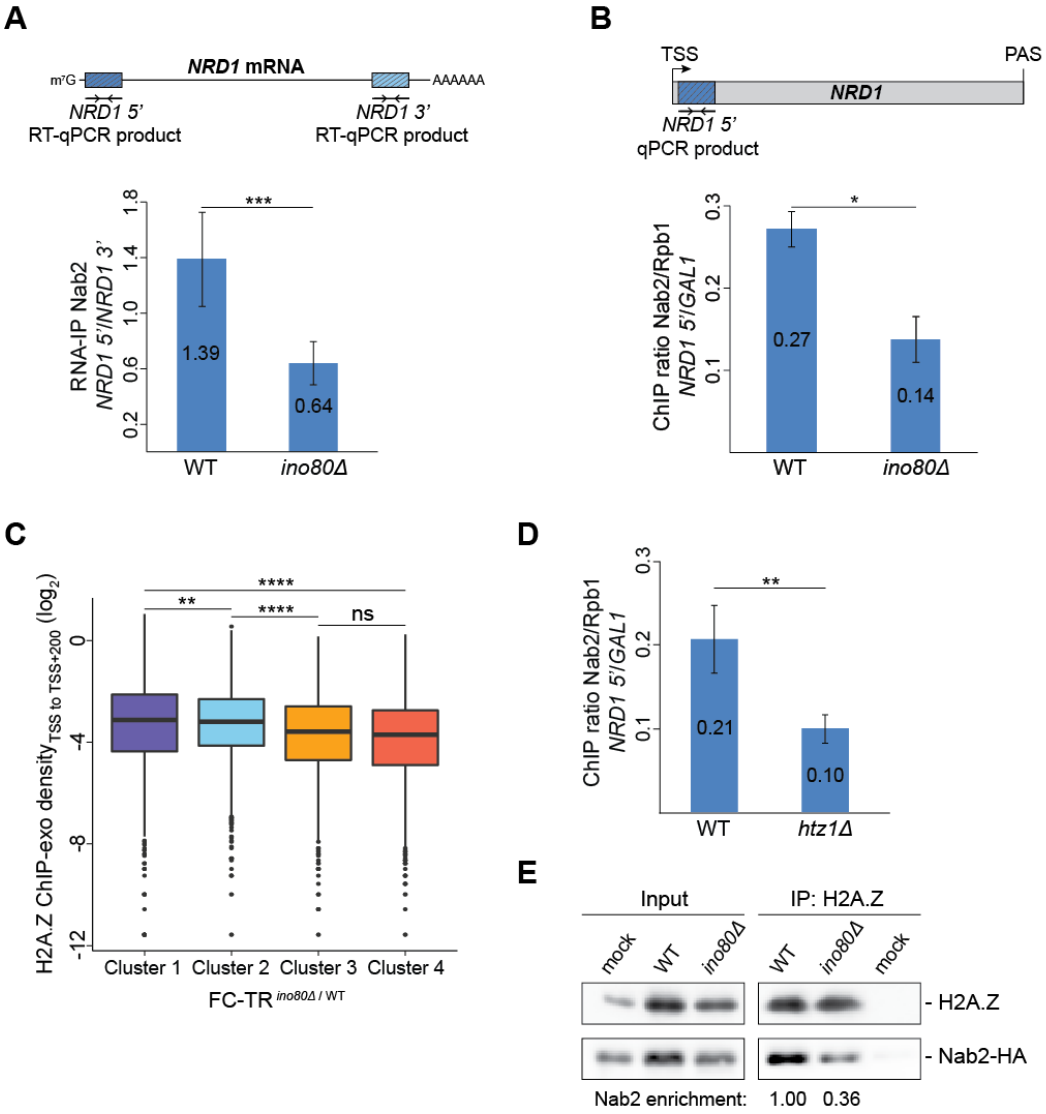
A
NRD1 mRNA
m7G
AAAAAA
NRD1 5'
RT-qPCR product
NRD1 3'
RT-qPCR product
RNA-IP Nab2
NRD1 5'/NRD1 3'
***
1.39
0.64
WT
ino80Δ
B
TSS
PAS
NRD1
NRD1 5'
qPCR product
ChIP ratio Nab2/Rpb1
NRD1 5'/GAL1
*
0.27
0.14
WT
ino80Δ
C
H2A.Z ChIP-exo density TSS to TSS+200 (log2)
****
**
****
ns
Cluster 1
Cluster 2
Cluster 3
Cluster 4
FC-TR ino80Δ / WT
D
ChIP ratio Nab2/Rpb1
NRD1 5'/GAL1
**
0.21
0.10
WT
htz1Δ
E
Input
IP: H2A.Z
mock
WT
ino80Δ
WT
ino80Δ
mock
- H2A.Z
- Nab2-HA
Nab2 enrichment: 1.00 0.36

Figure 6. Recruitment of Nab2 to chromatin and its association with H2A.Z depend on INO80.

(A) RNA immunoprecipitation for Nab2-HA in WT and *ino80Δ* cells. Ratio of binding of Nab2 to the promoter-proximal *NRD1* RNA (upper panel, *NRD1 5'*, dark blue) over binding to the 3' region of *NRD1* RNA (upper panel, *NRD1 3',* light blue) after correction for input, total RNA levels in the indicated strains. Bars, standard errors from four independent experiments. p-values were calculated by t-test after testing for normal distribution by Shapiro-Wilk test. ***, $p<0.001$.

(B) Chromatin immunoprecipitation for Nab2-HA and Rpb1 in WT and *ino80Δ* cells. Fold enrichment of each protein at the promoter-proximal region of *NRD1* gene (*NRD1 5'*) (upper panel, shaded in dark blue) was calculated relative to the *GAL1* promoter after correction for input DNA levels. ChIP ratio at the promoter-proximal region of *NRD1* gene (*NRD1 5'*) was calculated as Fold enrichment of Nab2-HA over Fold enrichment of Rpb1. Bars, standard errors from four independent experiments. p-values were calculated by t-test after testing for normal distribution by Shapiro-Wilk test. *, $p<0.05$.

(C) Boxplot analysis comparing published H2A.Z ChIP-exo densities (Yen et al., 2013) across mRNA genes clustered according to their relative FC-TR$^{ino80\Delta/\mathrm{WT}}$. p-values were calculated by Wilcoxon rank sum test. **, $p<0.01$. ****, $p<0.0001$. ns, non-significant.

(D) Chromatin immunoprecipitation for Nab2-HA and Rpb1 in WT and *htz1Δ* cells. Analysis was conducted as in (A). Bars, standard errors from three independent experiments. p-values were calculated by t-test after testing for normal distribution by Shapiro-Wilk test. **, $p<0.01$.

(E) Representative H2A.Z immunoprecipitation experiment. Nucleic acid-free lysates from WT and *ino80Δ* cells expressing Nab2-HA were subjected to H2A.Z-IP. Inputs and IP samples were immunoblotted for H2A.Z and HA. Nab2-HA enrichment in H2A.Z pulldowns is calculated as HA/H2A.Z IP ratio, corrected for the relative Nab2-HA abundance in the input samples. Nab2-

HA enrichment in WT is set arbitrarily to 1.0. All analysis was conducted from the same SDS-page gel.

See also Figure S6.

Figure 7

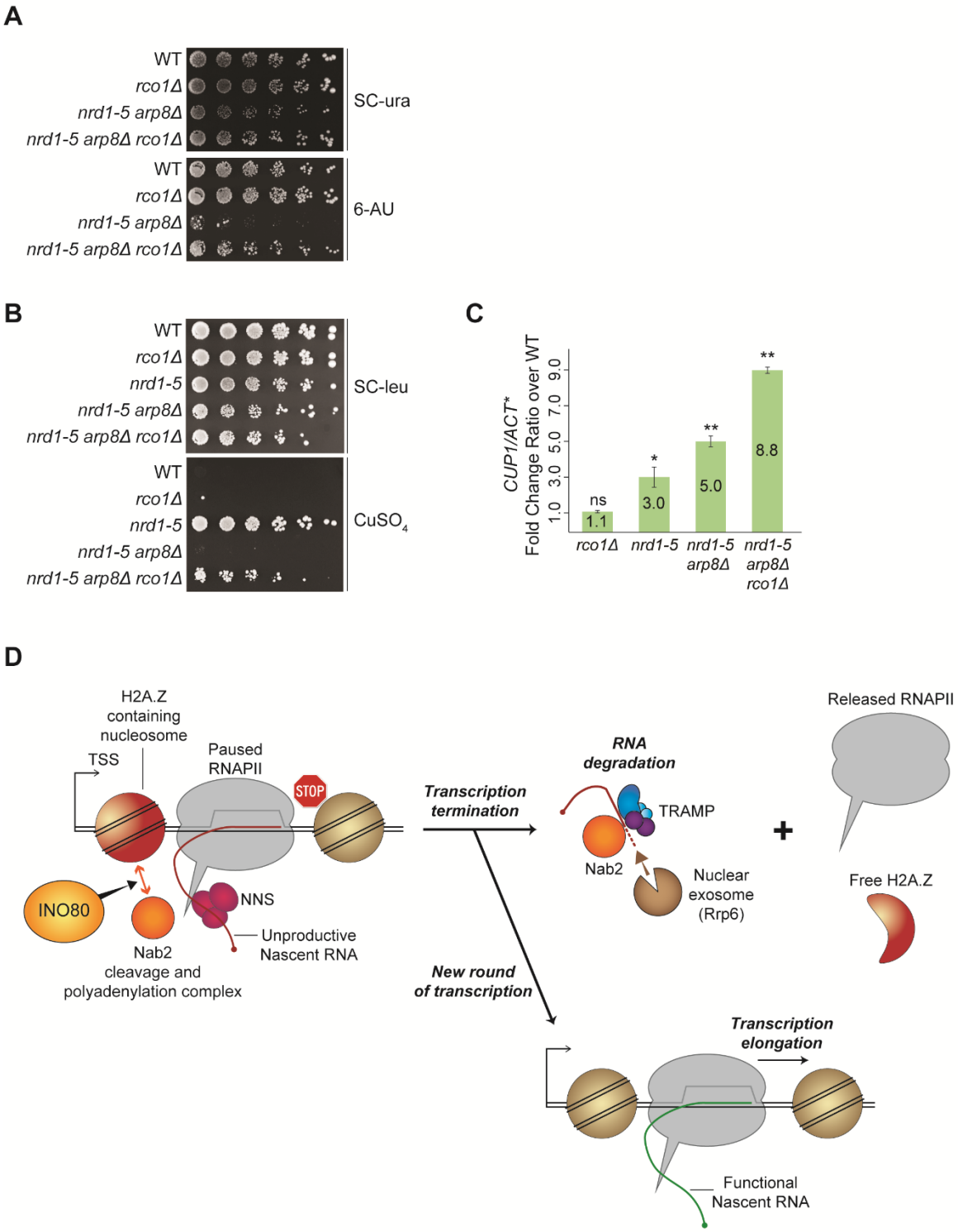
A
WT
rco1Δ
nrd1-5 arp8Δ
nrd1-5 arp8Δ rco1Δ
SC-ura
WT
rco1Δ
nrd1-5 arp8Δ
nrd1-5 arp8Δ rco1Δ
6-AU
B
WT
rco1Δ
nrd1-5
nrd1-5 arp8Δ
nrd1-5 arp8Δ rco1Δ
SC-leu
WT
rco1Δ
nrd1-5
nrd1-5 arp8Δ
nrd1-5 arp8Δ rco1Δ
CuSO4
C
CUP1/ACT*
Fold Change Ratio over WT
1.0
3.0
5.0
7.0
9.0
ns
1.1
*
3.0
**
5.0
**
8.8
rco1Δ
nrd1-5
nrd1-5 arp8Δ
nrd1-5 arp8Δ rco1Δ
D
H2A.Z containing nucleosome
TSS
Paused RNAPII
STOP
INO80
Nab2
cleavage and polyadenylation complex
NNS
Unproductive Nascent RNA
Transcription termination
RNA degradation
TRAMP
Nab2
Nuclear exosome (Rrp6)
Released RNAPII
Free H2A.Z
New round of transcription
Transcription elongation
Functional Nascent RNA

Figure 7. Deletion of *RCO1* rescues the defect in productive transcription caused by disruption of INO80.

(A) 5-fold serial dilution of cells from the indicated strains were plated onto both SC-ura and SC-ura + 50µg/ml 6-Azauracil (6-AU) and incubated at 30ºC for 4-5 days.

(B) 5-fold serial dilution of cells from the indicated strains were plated onto both SC-leu and SC-leu + 0.4mM $CuSO_4$ and incubated at 30ºC for 3 (SC-leu) and 7 days ($CuSO_4$). Pictures are representative of three independent experiments.

(C) RT-qPCR analysis for *CUP1* transcriptional read-through from the *ACT-CUP* reporter system in the indicated strains was conducted as in Figure 4E. Bars, standard errors from three independent experiments. p-values were calculated by t-test after testing for normal distribution by Shapiro-Wilk test. **, $p<0.01$. *, $p<0.05$. ns, non-significant.

(D) Model for INO80-dependent premature transcription termination. See Discussion for details.

See also Figure S7.

SUPPLEMENTARY FIGURES

Figure S1

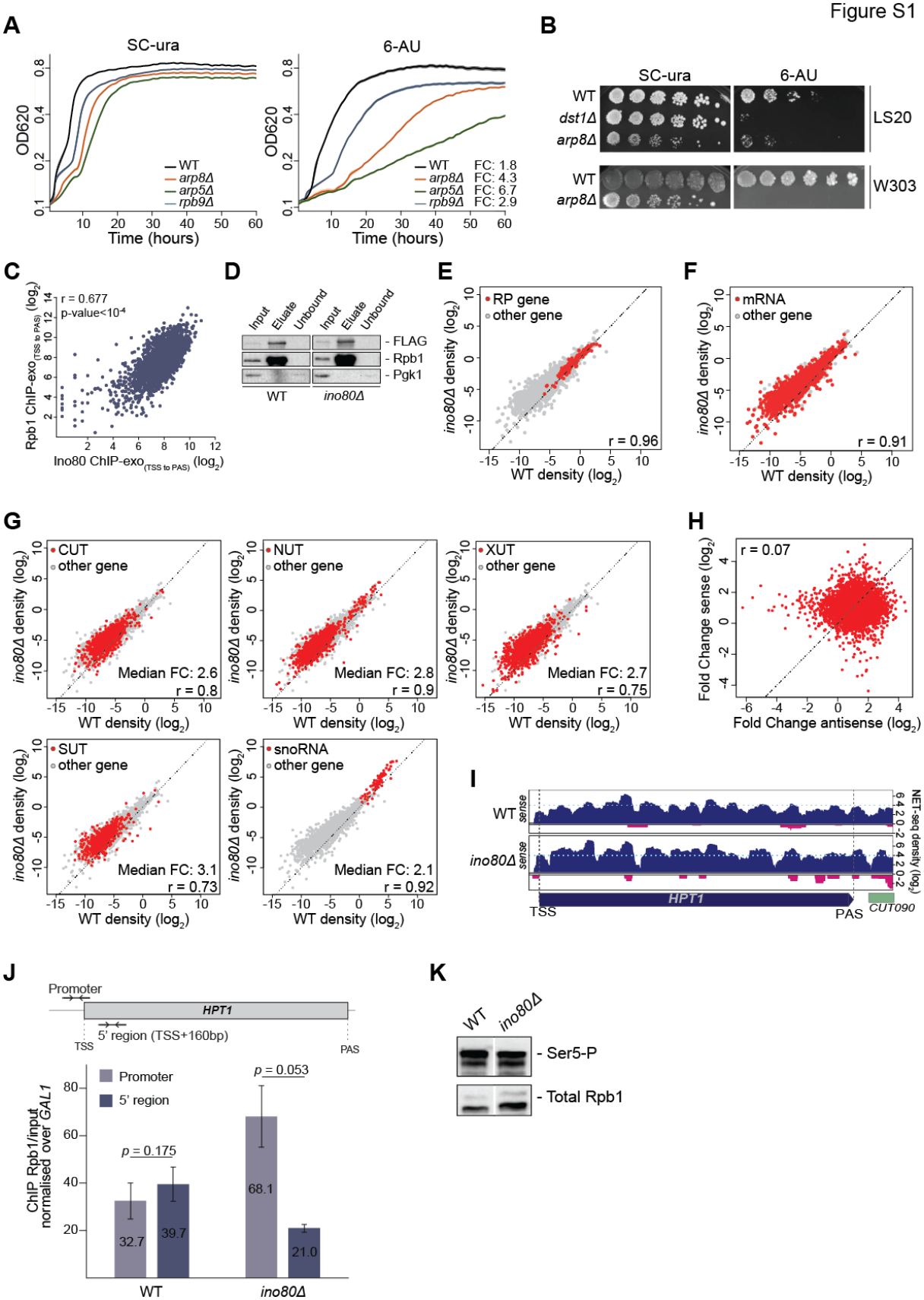
A
SC-ura
6-AU
OD620
Time (hours)
WT
arp8Δ
arp5Δ
rpb9Δ
FC: 1.8
FC: 4.3
FC: 6.7
FC: 2.9
B
SC-ura
6-AU
WT
dst1Δ
arp8Δ
LS20
WT
arp8Δ
W303
C
r = 0.677
p-value<10-4
Rpb1 ChIP-exo (TSS to PAS) (log2)
Ino80 ChIP-exo (TSS to PAS) (log2)
D
Input
Eluate
Unbound
- FLAG
- Rpb1
- Pgk1
WT
ino80Δ
E
RP gene
other gene
r = 0.96
ino80Δ density (log2)
WT density (log2)
F
mRNA
other gene
r = 0.91
G
CUT
NUT
XUT
SUT
snoRNA
other gene
Median FC: 2.6
r = 0.8
Median FC: 2.8
r = 0.9
Median FC: 2.7
r = 0.75
Median FC: 3.1
r = 0.73
Median FC: 2.1
r = 0.92
H
r = 0.07
Fold Change sense (log2)
Fold Change antisense (log2)
I
WT
ino80Δ
sense
NET-seq density (log2)
HPT1
TSS
PAS
CUT090
J
Promoter
HPT1
5' region (TSS+160bp)
TSS
PAS
Promoter
5' region
p = 0.053
p = 0.175
ChIP Rpb1/input normalised over GAL1
32.7
39.7
68.1
21.0
WT
ino80Δ
K
WT
ino80Δ
- Ser5-P
- Total Rpb1

Figure S1. Enrichment of nascent non-coding transcripts, accumulation of promoter-proximal nascent mRNA transcripts and defective transcriptional elongation in *ino80Δ*. *Related to Figure 1.*

(A) Cell proliferation analysis for the indicated strains grown exponentially in SC-ura (left panel) and in SC-ura containing 50µg/ml 6-azauracil (6-AU) (right panel) liquid media for the indicated time. Cell density was measured at OD^{620} and shown on a log_2 scale. Shading surrounding each line denotes standard error from four independent experiments. The mutant strain deleted for the RNA Polymerase II subunit Rpb9 (*rpb9Δ*) has reported transcriptional elongation defects in 6-AU (Hemming et al., 2000) and was used as control. Doubling time from OD^{620} 0.2 to OD^{620} 0.4 was calculated for all strains in both conditions. Fold Change ratio (FC) of doubling time in 6-AU over SC-ura is shown (right panel).

(B) 5-fold serial dilution of cells from the indicated strains were plated onto both SC-ura and SC-ura + 50µg/ml 6-Azauracil (6-AU) and incubated at 30ºC for 4-5 days. Genetic backgrounds (LS20, W303) are indicated. The mutant strain deleted for the Dst1/TFIIS transcription elongation factor (*dst1Δ*) was used as control (Riles et al., 2004).

(C) Scatterplot analysis comparing Ino80 (Yen et al., 2013) and Rpb1 ChIP-exo densities between the transcription start site and polyadenylation site (TSS to PAS) in the 5798 mRNA yeast genes. Pearson's correlation coefficient (r) and p-value are indicated.

(D) Rpb1-FLAG is efficiently immunoprecipitated from yeast cells during NET-seq analysis. Lysates from WT and *ino80Δ* cells expressing *RPB1-FLAG* were subjected to FLAG immunoprecipitation using FLAG beads. Rpb1-FLAG was subsequently eluted from the beads with FLAG peptide. Input, eluate and unbound samples were immunoblotted against FLAG epitope and total Rpb1. Immunoblotting against Pgk1 serves as loading control. All samples were resolved in the same SDS-page gel.

(E) Scatterplot analysis comparing NET-seq densities in WT and *ino80Δ* for Ribosomal Protein (RP) mRNA yeast genes after normalization over the average NET-seq density of ribosomal protein (RP) genes plotted on a $\log_2$ scale. The Pearson's correlation coefficient (r) is indicated.

(F) Scatterplot analysis comparing NET-seq densities in WT and *ino80Δ* for mRNA genes after normalization over the average NET-seq density of ribosomal protein (RP) genes, plotted on a $\log_2$ scale. The Pearson's correlation coefficient (r) is indicated.

(G) Scatterplot analysis comparing NET-seq densities in WT and *ino80Δ* for CUT, NUT, XUT, SUT and snoRNA yeast genes plotted on a $\log_2$ scale. Pearson's correlation coefficient (r) and median *ino80Δ*/WT fold-change (Median FC) are indicated.

(H) Scatterplot analysis comparing the changes in NET-seq densities between WT and *ino80Δ* (Fold-Change) for sense transcripts and their relative antisense transcripts over mRNA gene regions, plotted on a $\log_2$ scale. Pearson's correlation coefficient (r) is indicated.

(I) NET-seq density profiles in WT and *ino80Δ* for sense and antisense transcripts across the *HPT1* mRNA gene region plotted with VING software (Descrimes et al., 2015).

(G) Chromatin immunoprecipitation for Rpb1 in WT and *ino80Δ* cells. Rpb1 enrichment was measured at either the promoter (Promoter) or the promoter-proximal region (5' region) of the *HPT1* mRNA gene and normalised to the *GAL1* promoter, after correction for input DNA levels. Bars, standard errors from three independent experiments. p-values were calculated by t-test after testing for normal distribution by Shapiro-Wilk test.

(K) Nucleic-acid free lysates from WT and *ino80Δ* cells were subjected to immunoblotting against Ser5-phosphorylated C-terminal domain of Rpb1 (Ser5-P) and Total Rpb1. All samples were resolved in the same SDS-page gel.

Figure S2

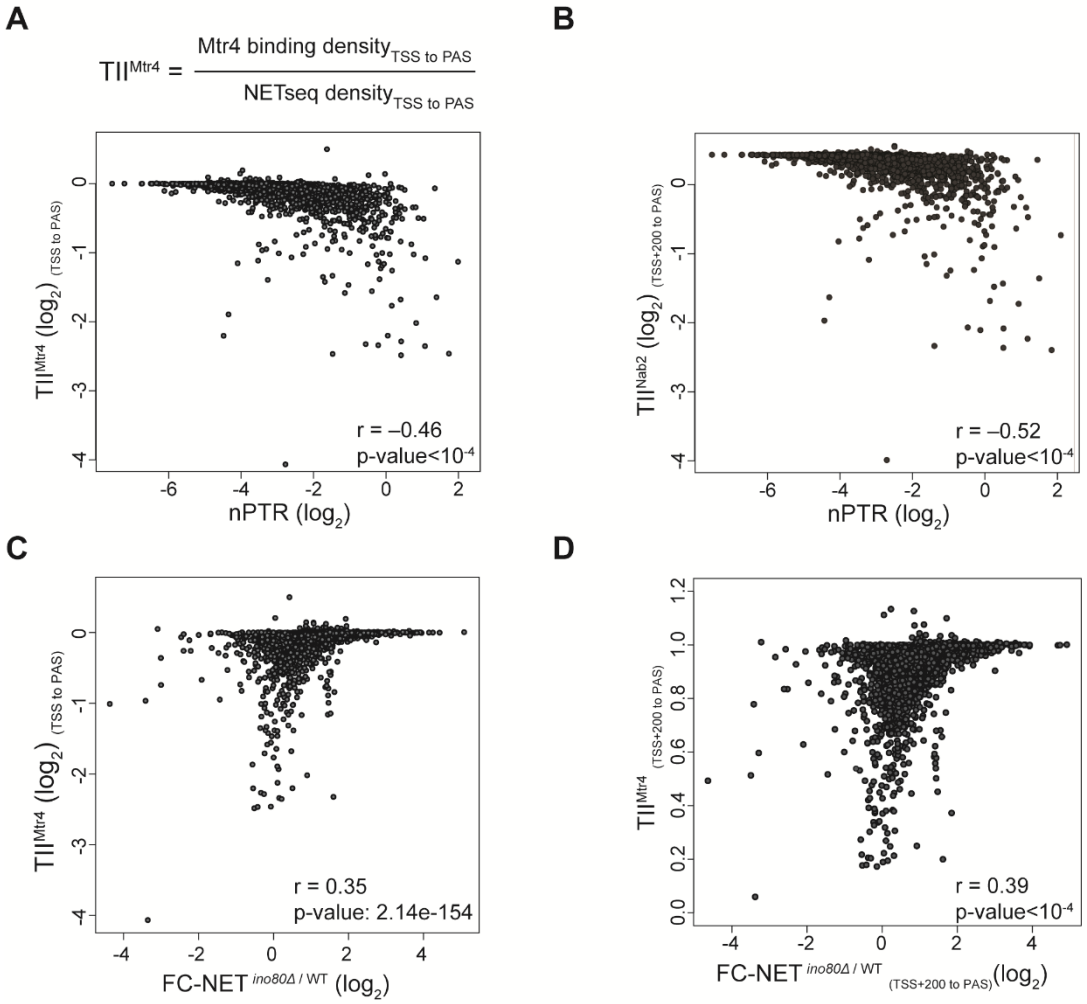
A
TII^Mtr4 = Mtr4 binding density_TSS to PAS / NETseq density_TSS to PAS
TII^Mtr4 (log2) (TSS to PAS)
nPTR (log2)
r = –0.46
p-value<10^-4
B
TII^Nab2 (log2) (TSS+200 to PAS)
nPTR (log2)
r = –0.52
p-value<10^-4
C
TII^Mtr4 (log2) (TSS to PAS)
FC-NET ino80Δ / WT (log2)
r = 0.35
p-value: 2.14e-154
D
TII^Mtr4 (TSS+200 to PAS)
FC-NET ino80Δ / WT (TSS+200 to PAS)(log2)
r = 0.39
p-value<10^-4

Figure S2. Accumulation of nascent mRNA transcripts in *ino80Δ* is associated with increased RNA quality control. ***Related to Figure 2.***

(A) Upper panel, formula for calculating the Mtr4 Transcription Instability Index (TII^{Mtr4}) from Mtr4 CRAC (Tuck and Tollervey, 2013) and NET-seq densities. Bottom panel, scatter plot analysis comparing TII^{Mtr4} and nascent Productive Transcriptional Rates (nPTR) (Pelechano et al., 2010) over mRNA genes (TSS to PAS), shown on a log_2 scale. Pearson's correlation coefficient (r) and p-value are indicated.

(B) scatter plot analysis comparing TII^{Nab2} and nascent Productive Transcriptional Rates (nPTR) (Pelechano et al., 2010) across mRNA gene regions comprised between 200bp downstream of transcription start site (TSS+200bp) and the polyadenylation site (PAS). Data shown on a log_2 scale. Pearson's correlation coefficient (r) and p-value are indicated.

(C) Scatterplot analysis comparing TII^{Mtr4} and the *ino80Δ*/WT NET-seq density Fold Change ($FC\text{-}NET^{ino80\Delta/WT}$). Data are shown on a log_2 scale. Pearson's correlation coefficient (r) and p-value are indicated.

(D) Scatterplot analysis comparing TII^{Mtr4} and the *ino80Δ*/WT NET-seq density Fold Change ($FC\text{-}NET^{ino80\Delta/WT}$) across mRNA gene regions comprised between 200bp downstream of transcription start site (TSS+200bp) and the polyadenylation site (PAS). Pearson's correlation coefficient (r) and p-value are indicated.

Figure S3

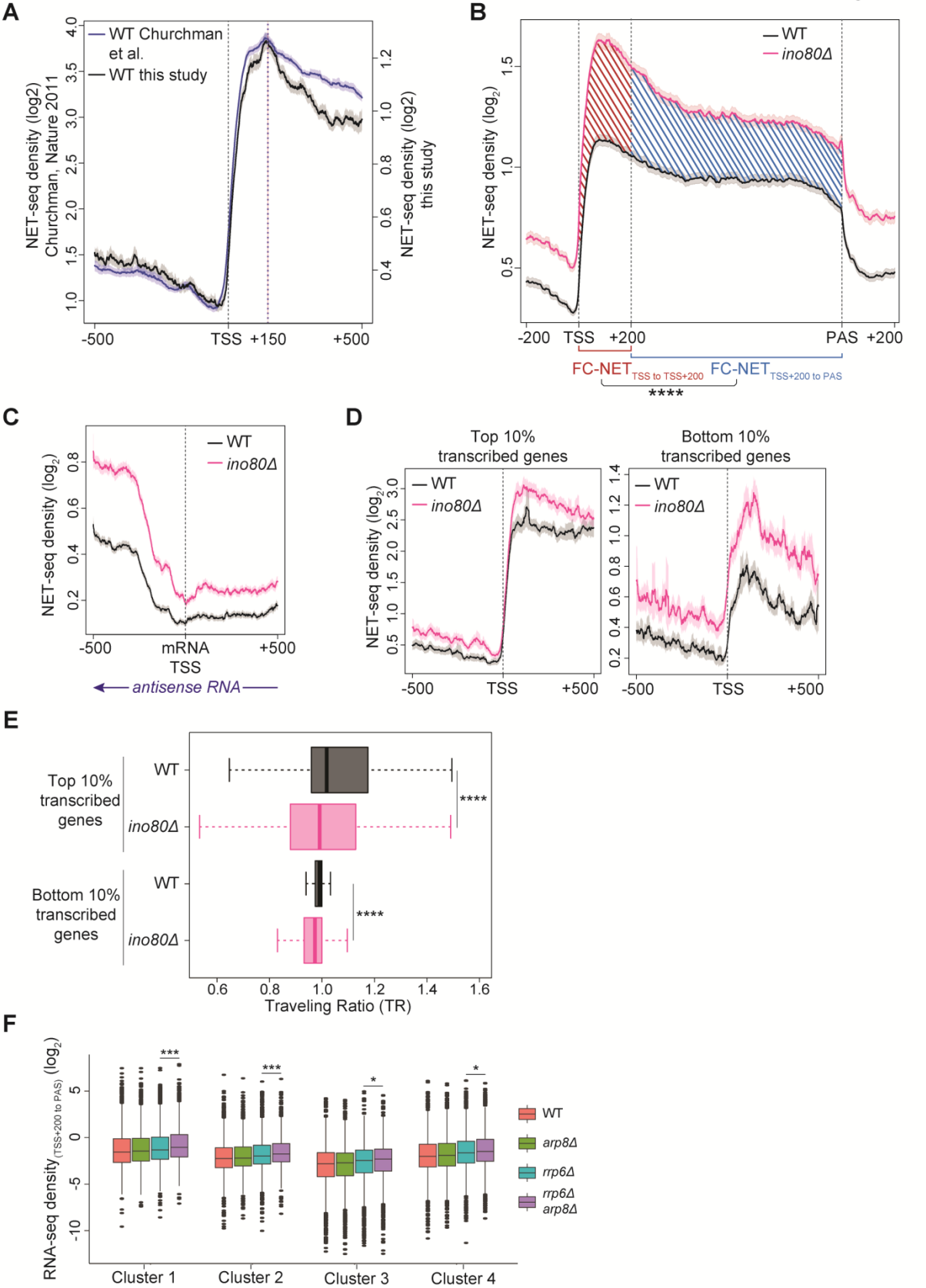
A
WT Churchman et al.
WT this study
NET-seq density (log2) Churchman, Nature 2011
NET-seq density (log2) this study
-500
TSS +150
+500
B
WT
ino80Δ
NET-seq density (log2)
-200 TSS +200
PAS +200
FC-NET TSS to TSS+200
FC-NET TSS+200 to PAS
****
C
WT
ino80Δ
NET-seq density (log2)
-500
mRNA TSS
+500
antisense RNA
D
Top 10% transcribed genes
Bottom 10% transcribed genes
WT
ino80Δ
NET-seq density (log2)
-500
TSS
+500
E
Top 10% transcribed genes
Bottom 10% transcribed genes
WT
ino80Δ
****
Traveling Ratio (TR)
F
RNA-seq density (TSS+200 to PAS) (log2)
WT
arp8Δ
rrp6Δ
rrp6Δ arp8Δ
Cluster 1
Cluster 2
Cluster 3
Cluster 4

Figure S3. INO80 regulates promoter-proximal pausing of RNAPII. ***Related to Figure 3.***

(A) Metagene analysis of NET-seq density profiles from the Churchman *et al.* study (Churchman and Weissman, 2011) and from this study averaged across mRNA genes in WT. Tags were aligned relative to TSS and plotted on a $\log_2$ scale. Blue vertical line marks the +150bp location relative to TSS.

(B) Schematic representation of the significance difference between changes in nascent transcription in *ino80Δ* compared to WT over gene bodies (FC-$NET_{TSS+200\ to\ PAS}$) and over the 200bp region downstream of TSS (FC-$NET_{TSS\ to\ TSS+200}$). p-value was calculated by Wilcoxon rank-sum test. ****, $p < 0.0001$.

(C) Metagene analysis of NET-seq density profiles for antisense to mRNA transcripts for WT and *ino80Δ*. Tags were aligned relative to the sense TSS and plotted on a $\log_2$ scale. Arrow indicates the 5' to 3' direction of the antisense transcripts.

(D) Metagene analysis of NET-seq density profiles for WT and *ino80Δ* averaged across the 10% most highly (left panel) and 10% most lowly (right panel) expressed mRNA genes derived from (Nagalakshmi et al., 2008). Tags were aligned relative to TSS and plotted on $\log_2$ scale.

(E) Boxplot analysis for Traveling Ratio for the 10% most highly (*top*) and 10% most lowly (*bottom*) expressed mRNA genes in WT and *ino80Δ*. p-value was calculated by Wilcoxon rank-sum test. ****, $p < 0.0001$.

(F) Boxplot analysis comparing RNA-seq densities from the indicated strains across the mRNA gene body region from TSS+200bp to PAS in the four gene clusters defined by their relative FC-$TR^{ino80\Delta/WT}$. p-values were calculated by Wilcoxon rank-sum test. ***, $p<0.001$. **, $p<0.01$.

Figure S4

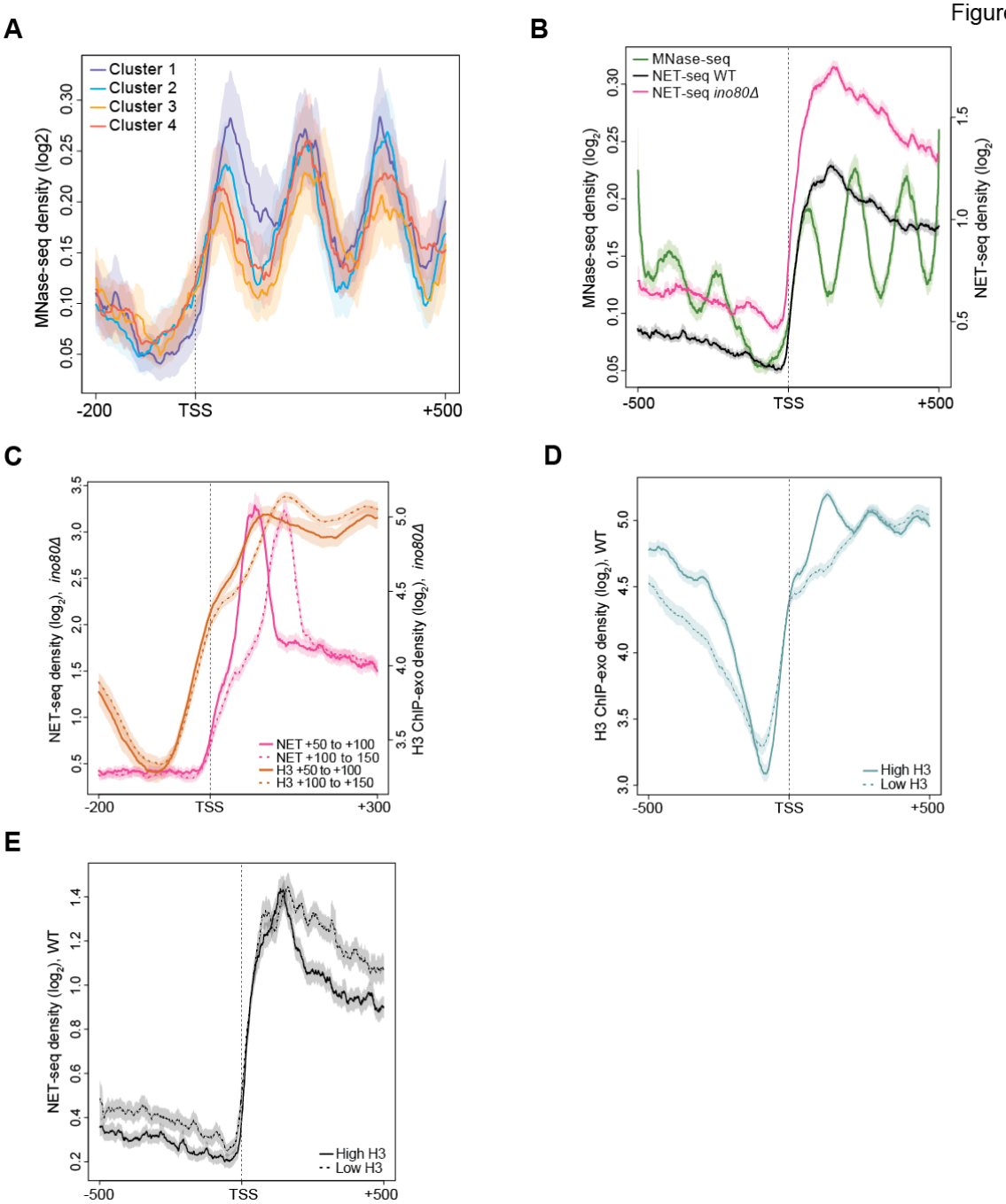
A
Cluster 1
Cluster 2
Cluster 3
Cluster 4
MNase-seq density (log2)
0.05
0.10
0.15
0.20
0.25
0.30
-200
TSS
+500
B
MNase-seq
NET-seq WT
NET-seq ino80Δ
MNase-seq density (log2)
NET-seq density (log2)
-500
TSS
+500
C
NET-seq density (log2), ino80Δ
H3 ChIP-exo density (log2), ino80Δ
NET +50 to +100
NET +100 to 150
H3 +50 to +100
H3 +100 to +150
-200
TSS
+300
D
H3 ChIP-exo density (log2), WT
High H3
Low H3
-500
TSS
+500
E
NET-seq density (log2), WT
High H3
Low H3
-500
TSS
+500

Figure S4. The role of INO80 in RNA quality control is associated with H3 binding to DNA. ***Related to Figure 4.***

(A) Metagene analyses MNase-seq density profiles from (Yen et al., 2012) in WT in the four gene clusters defined by their relative FC-TR$^{ino80\Delta/\mathrm{WT}}$ (Figure 3C). Tags were aligned relative to TSS and plotted on a $\log_2$ scale.

(B) Metagene analysis for NET-seq density profiles for WT and *ino80Δ* and MNase-seq density profile for WT from (Yen et al., 2012) averaged across mRNA genes. Tags were aligned relative to TSS and plotted on a $\log_2$ scale.

(C) Metagene analysis for NET-seq and histone H3 ChIP-exo density profiles in *ino80Δ* for mRNA gene clusters with maximum peak of NET-seq density either between +50 and +100bp (solid lines, 501 genes), or between +100 and +150bp (broken lines, 501 genes) from TSS. Data plotted on a $\log_2$ scale.

(D) Metagene analysis for ChIP-exo density profiles for histone H3 in WT for the mRNA genes with highest and lowest H3 enrichment in the +1/+2 linker using 30th percentile cutoff. Data plotted on a $\log_2$ scale. Gene lists for 30th percentile cutoff derived from (Rhee et al., 2014).

(E) Metagene analysis for NET-seq density profiles in WT for the mRNA genes with highest and lowest H3 enrichment in the +1/+2 linker using 30th percentile cutoff described in (C). Data plotted on a $\log_2$ scale.

Figure S5

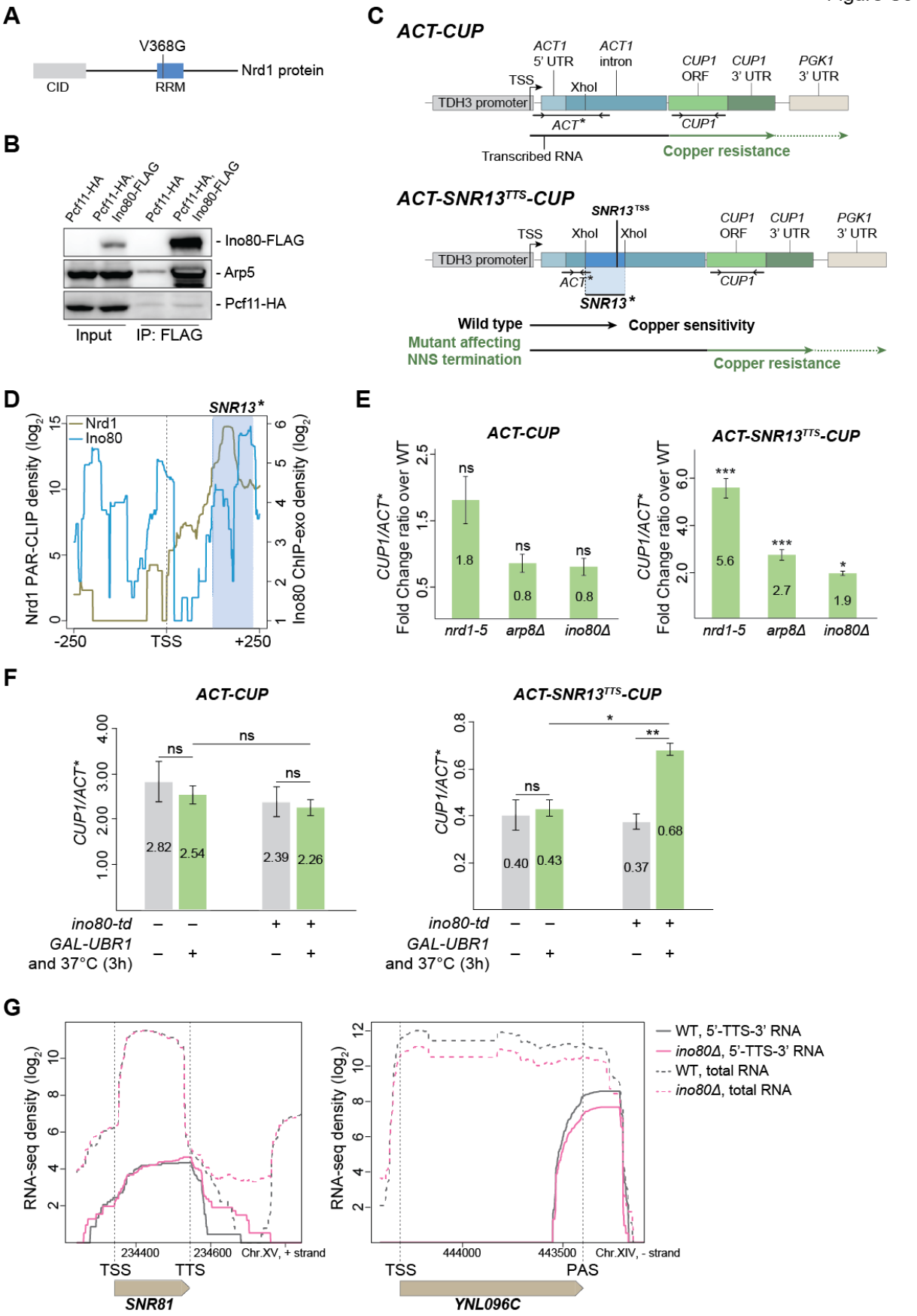
A
V368G
Nrd1 protein
CID
RRM
B
Pcf11-HA
Pcf11-HA, Ino80-FLAG
Pcf11-HA
Pcf11-HA, Ino80-FLAG
- Ino80-FLAG
- Arp5
- Pcf11-HA
Input
IP: FLAG
C
ACT-CUP
ACT1 5' UTR
ACT1 intron
CUP1 ORF
CUP1 3' UTR
PGK1 3' UTR
TSS
XhoI
TDH3 promoter
ACT*
CUP1
Transcribed RNA
Copper resistance
ACT-SNR13TTS-CUP
SNR13TSS
TSS
XhoI
XhoI
CUP1 ORF
CUP1 3' UTR
PGK1 3' UTR
TDH3 promoter
ACT*
CUP1
SNR13*
Wild type
Copper sensitivity
Mutant affecting NNS termination
Copper resistance
D
SNR13*
Nrd1
Ino80
Nrd1 PAR-CLIP density (log2)
Ino80 ChIP-exo density (log2)
-250
TSS
+250
E
ACT-CUP
ACT-SNR13TTS-CUP
CUP1/ACT* Fold Change ratio over WT
ns
1.8
0.8
0.8
***
5.6
***
2.7
*
1.9
nrd1-5
arp8Δ
ino80Δ
F
ACT-CUP
ACT-SNR13TTS-CUP
CUP1/ACT*
ns
2.82
2.54
2.39
2.26
0.40
0.43
0.37
0.68
*
**
ino80-td
GAL-UBR1
and 37°C (3h)
G
RNA-seq density (log2)
234400
234600
Chr.XV, + strand
TSS
TTS
SNR81
444000
443500
Chr.XIV, - strand
TSS
PAS
YNL096C
WT, 5'-TTS-3' RNA
ino80Δ, 5'-TTS-3' RNA
WT, total RNA
ino80Δ, total RNA

Figure S5. INO80 is involved in NNS-dependent termination. ***Related to Figure 5.***

(A) Schematic representation of Nrd1 protein structure in the *nrd1-5* mutant strain. CID, Rpb1 CTD-Interacting Domain. RRM, RNA Recognition Motif. V368G, substitution of Valine-368 with Glycine in the RNA-binding face of the RNA recognition motif (RRM) (Bacikova et al., 2014).

(B) Nucleic acid-free lysates from cells co-expressing Pcf11-HA with Ino80 either untagged or tagged with FLAG epitope were subjected to FLAG-IP. Inputs and IP samples were immunoblotted for FLAG, Arp5 and HA. Samples were resolved in the same SDS-page gel.

(C) Schematic representation of the *ACT-CUP* (pGAC24) and *ACT-SNR^{TTS}-CUP* (pGAC24-SNR13^{TTS}) reporter systems for transcription termination reported in (Steinmetz et al., 2001). The regions amplified by RT-qPCR for *ACT** and *CUP1* are underlined. The region of the *SNR13* gene between +125 to +232bp from TSS that was cloned in the *ACT-SNR13^{TTS}-CUP* plasmid (Steinmetz et al., 2001) is shaded in blue (*SNR13**). The expected phenotype of cells transformed with either the *ACT-CUP* or the *ACT-SNR13^{TTS}-CUP* plasmid is shown.

(D) Snapshot of Nrd1 PAR-CLIP density profile from (Creamer et al., 2011) and Ino80 ChIP-exo density profile from (Yen et al., 2013) across the *SNR13* snoRNA gene. Tags were aligned relative to TSS and plotted on a $\log_2$ scale. The region between +125 to +232bp from TSS cloned in the *ACT-SNR13^{TTS}-CUP* plasmid described in (C) (Steinmetz et al., 2001) is highlighted in blue (*SNR13**).

(E) RT-qPCR analysis for the *CUP1/ACT** ratio was conducted in the indicated strains transformed with either the *ACT-CUP* (left panel) or *ACT-SNR^{TTS}-CUP* (right panel) plasmids. Bars, standard errors from three independent experiments. Asterisks indicate statistical significance of the change in the respective mutant compared to the WT as calculated by t-test. ns: non-significant. *, $p<0.05$. ***, $p<0.001$.

(F) RT-qPCR analysis was conducted in both WT and the *ino80-td* degron-inducible strain (Jonsson et al., 2004) transformed with the *ACT-CUP* control plasmid described in (C). Galactose-induced activation for 3 hours at 37ºC (+) and glucose-induced suppression (–) of the *UBR1* N-recognin in the two strains is indicated. Bars, standard errors from four independent experiments. p-values were calculated by t-test after testing for normal distribution by Shapiro-Wilk test. ns, non-significant.

(G) Snapshots representing RNA-seq densities in WT and *ino80Δ* across the snoRNA genes *SNR47* and *SNR81*, and the ribosomal protein coding gene YNL096C. Solid lines, density of reads encompassing the transcription termination site (5'-TTS-3') as described in Figure 4F. Analysis for the *YNL096C* was performed around the polyadenylation site (PAS). Broken lines, total RNA-seq density. Genomic coordinates of Chromosome XV around the *SNR47* gene, and of Chromosome XVI around the *YNL096C* gene are shown. The closest gene downstream of *SNR81* (coordinates: 234346 to 234546) is *GAL11* (TSS: Chromosome XV, 234940). The closest gene downstream of *YNL096C* is the *PHO23* mRNA gene (TSS: Chromosome XIV, 442509).

Figure S6

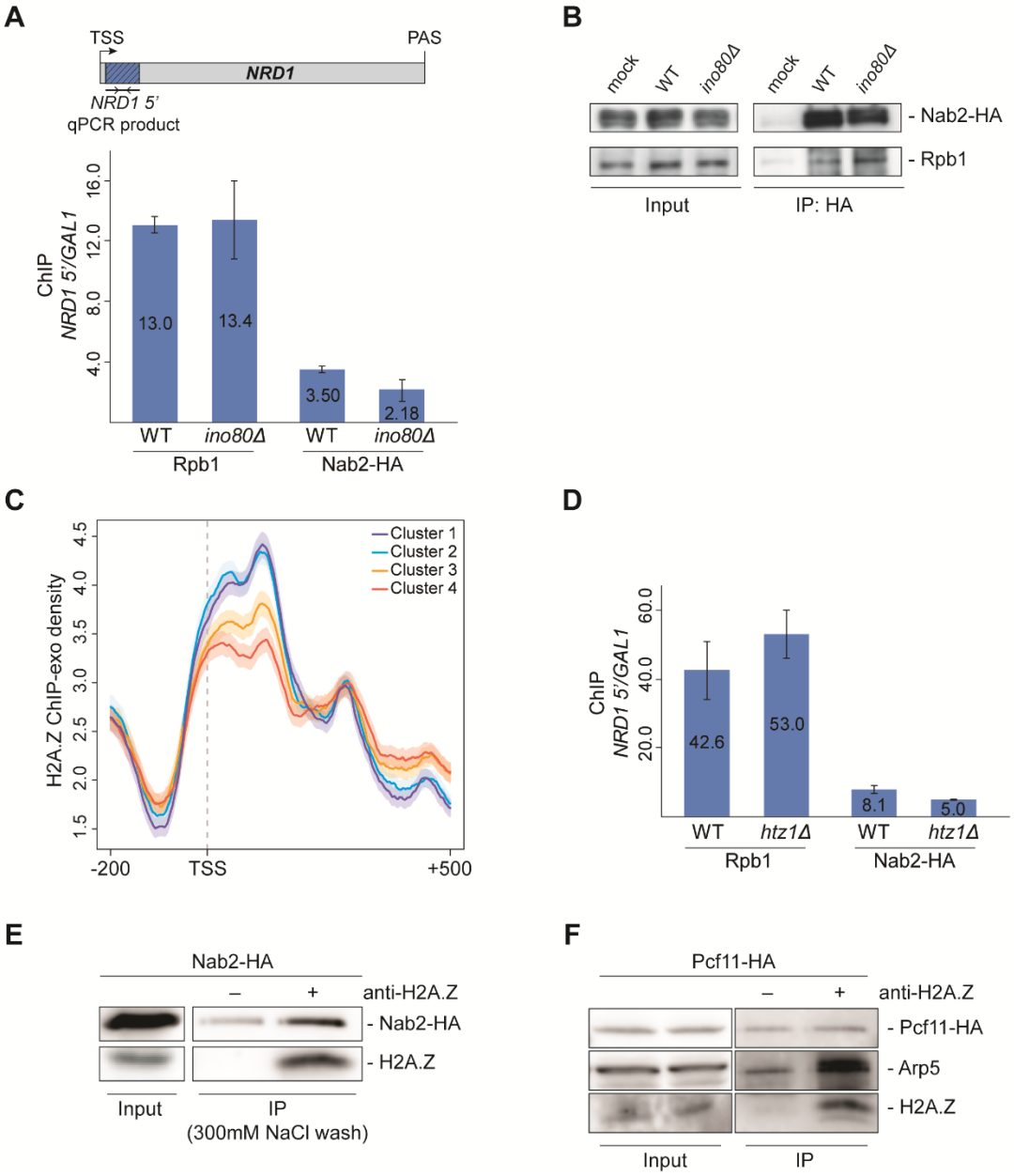
A
TSS
PAS
NRD1
NRD1 5'
qPCR product
ChIP
NRD1 5'/GAL1
16.0
12.0
8.0
4.0
13.0
13.4
3.50
2.18
WT
ino80Δ
WT
ino80Δ
Rpb1
Nab2-HA
B
mock
WT
ino80Δ
mock
WT
ino80Δ
- Nab2-HA
- Rpb1
Input
IP: HA
C
H2A.Z ChIP-exo density
4.5
4.0
3.5
3.0
2.5
2.0
1.5
Cluster 1
Cluster 2
Cluster 3
Cluster 4
-200
TSS
+500
D
ChIP
NRD1 5'/GAL1
60.0
40.0
20.0
42.6
53.0
8.1
5.0
WT
htz1Δ
WT
htz1Δ
Rpb1
Nab2-HA
E
Nab2-HA
–
+
anti-H2A.Z
- Nab2-HA
- H2A.Z
Input
IP
(300mM NaCl wash)
F
Pcf11-HA
–
+
anti-H2A.Z
- Pcf11-HA
- Arp5
- H2A.Z
Input
IP

Figure S6. INO80 and H2A.Z are involved in premature transcription termination. ***Related to Figure 6.***

(A) Chromatin immunoprecipitation for Nab2-HA and Rpb1 in WT and *ino80Δ* cells. Fold enrichment analysis at the promoter-proximal region of *NRD1* gene (*NRD1 5'*) (upper panel, shaded in dark blue) was conducted as Figure 6B.

(B) Nucleic acid-free lysates from WT and *ino80Δ* cells both expressing Nab2-HA were subjected to HA-IP. Inputs and IP samples were immunoblotted for Rpb1 and HA. Mock, WT protein lysate subjected to immunoprecipitation with a control IgG antibody.

(C) Metagene analyses for H2A.Z ChIP-seq (Yen et al., 2013) in WT cells in the four gene clusters defined by their relative FC-TR$^{ino80\Delta/\mathrm{WT}}$. Tags were aligned relative to TSS.

(D) Chromatin immunoprecipitation analysis for Nab2-HA and Rpb1 in WT and *htz1Δ*. Fold enrichment analysis at the promoter-proximal region of *NRD1* gene (*NRD1 5'*) was conducted as Figure 6A.

(E), Nucleic acid-free lysates from WT cells expressing Nab2-HA were subjected to immunoprecipitation with either an anti-H2A.Z antibody (+) or a non-specific IgG antibody as a control (–), then washed in the presence of 300mM NaCl. Inputs and IP samples were immunoblotted for HA and H2A.Z. All analysis was conducted from the same SDS-page gel.

(F) Nucleic acid-free lysates from cells expressing Pcf11-HA were subjected to immunoprecipitation with either an anti-H2A.Z antibody (+) or a non-specific IgG antibody as a control (–). Inputs and IP samples were immunoblotted for HA, Arp5 and H2A.Z. The western for Pcf11-HA was over-exposed in order to detect the background levels of Pcf11 binding to the beads. All analysis was conducted from the same SDS-page gel.

Figure S7

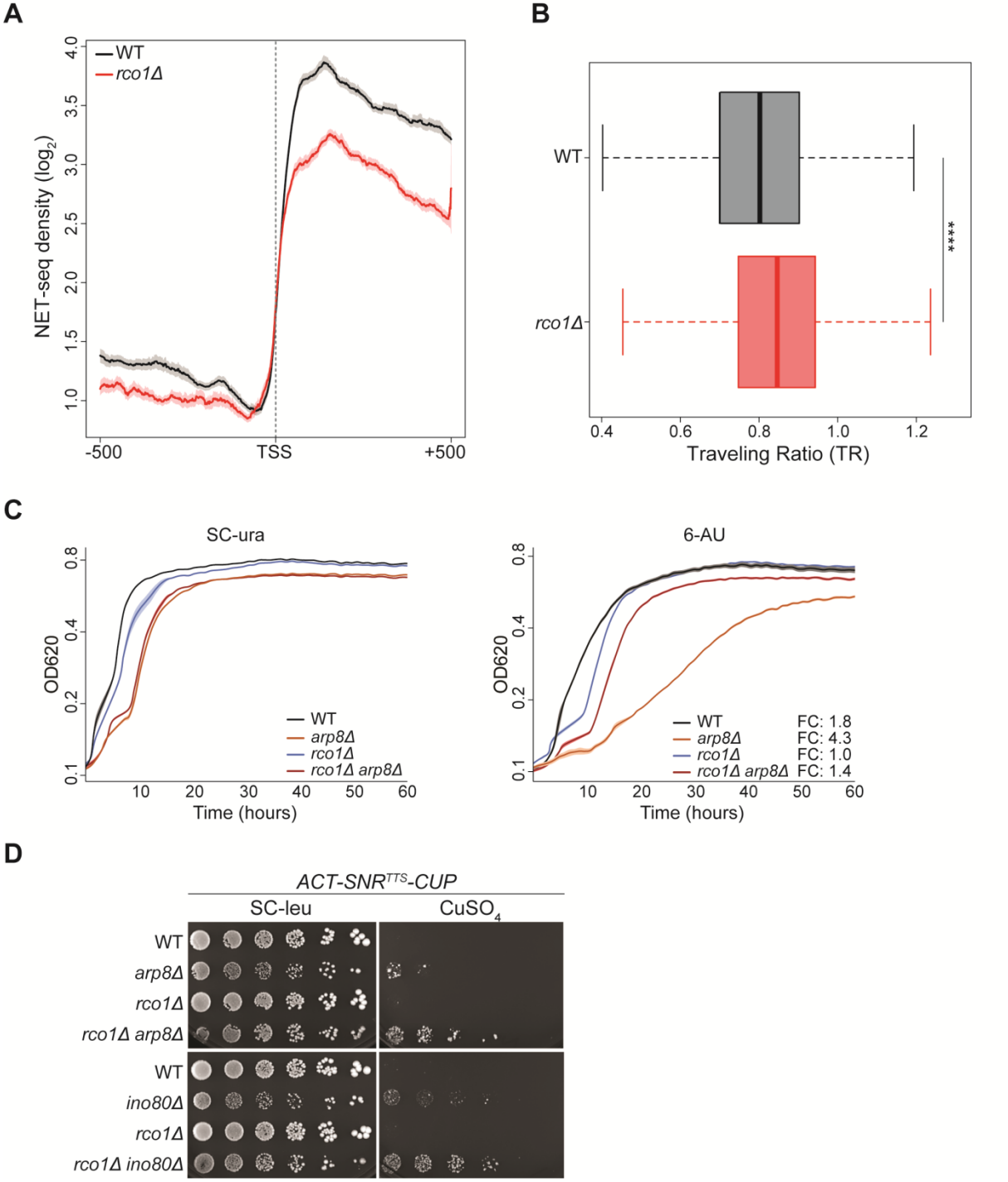
A
WT
rco1Δ
NET-seq density (log2)
4.0
3.5
3.0
2.5
2.0
1.5
1.0
-500
TSS
+500
B
WT
rco1Δ
****
0.4
0.6
0.8
1.0
1.2
Traveling Ratio (TR)
C
SC-ura
OD620
0.8
0.4
0.2
0.1
WT
arp8Δ
rco1Δ
rco1Δ arp8Δ
10
20
30
40
50
60
Time (hours)
6-AU
OD620
0.8
0.4
0.2
0.1
WT FC: 1.8
arp8Δ FC: 4.3
rco1Δ FC: 1.0
rco1Δ arp8Δ FC: 1.4
10
20
30
40
50
60
Time (hours)
D
ACT-SNRTTS-CUP
SC-leu
CuSO4
WT
arp8Δ
rco1Δ
rco1Δ arp8Δ
WT
ino80Δ
rco1Δ
rco1Δ ino80Δ

Figure S7. Deletion of *RCO1* alleviates accumulation of promoter-proximal nascent mRNA transcripts and enhances transcriptional elongation. ***Related to Figure 7.***

(A) Metagene analysis for NET-seq density profiles for WT and *rco1Δ* from (Churchman and Weissman, 2011) averaged across all mRNA genes. Data plotted on a $\log_2$ scale.

(B) Boxplot analysis for Traveling Ratio for mRNA genes in WT and *rco1Δ* as detailed in Figure 3B. TR was calculated from (Churchman and Weissman, 2011). P-value was calculated by Wilcoxon rank-sum test. ****, $p<0.0001$.

(C) Cell proliferation analysis for the indicated strains grown exponentially in SC-ura (left panel) and in SC-ura liquid media containing 50ug/ml 6-azauracil (6-AU) (right panel) for the indicated time. Cell density was measured at OD^{620} and is shown on a $\log_2$ scale. Shading surrounding each line denotes standard error from four independent experiments. Doubling time from OD^{620} 0.25 to OD^{620} 0.5 was calculated for all strains in both conditions. Fold Change ratio (FC) of doubling time in 6-AU over SC-ura is shown (right panel).

(D) 5-fold serial dilution of cells from the indicated strains transformed with the *ACT-SNR13^{TTS}-CUP* plasmid (Figure S4C) were plated onto SC-leu and SC-leu + 0.4mM $CuSO_4$ and incubated at 30°C for 5-7 days.

Supplementary Table 1 - Yeast strains used in this study

Strain	Genotype	Reference/Source
YM50	LS20 [*Mat*Δ *ade2 can1r cyh2r lys S URA3-52 trp1*Δ *his3-*Δ*200GAL:HO leu 2*Δ]	(Sandell and Zakian, 1993)
YM85	LS20 *ino80*Δ*::KANMX*	(Papamichos-Chronakis and Peterson, 2008)
YM166	LS20 *htz1*Δ*::hisG-ura3*Δ *HTZ1::URA3*	(Papamichos-Chronakis et al., 2011)
YM167	LS20 *htz1*Δ*::hisG-ura3*Δ *HTZ1::URA3 ino80*Δ*::KANMX*	(Papamichos-Chronakis et al., 2011)
YM181	LS20 *arp8*Δ*::KANMX*	(Papamichos-Chronakis et al., 2011)
YM311	W303 [*MATa ade2-1 can1-100 his3-11 leu2,3,112 trp1-1 ura3-1*]	(Verma et al., 2011)
YM334	W303 *arp8*Δ*::KANMX*	(Lafon et al., 2015b)
YM467	LS20 *dst1*Δ*::KANMX*	This study
YM468	LS20 *rpb9*Δ*::KANMX*	This study
YM498	LS20 *rco1*Δ*::HPHMX*	This study
YM499	LS20 *rco1*Δ*::HPHMX arp8*Δ*::KANMX*	This study
YM500	LS20 *rco1*Δ*::HPHMX ino80*Δ*::KANMX*	This study
YM753	BY4741 [*MATa his3Δ1 leu2Δ0 met15Δ0 ura3Δ0*] *NRD1-3XHA::HIS3*	This study
YM801	46a [*MATa ura3 his3 trp1 lys2 ade2 leu2 cup1Δ*]	(Steinmetz and Brow, 1996)
YM802	46a *nrd1-5*	(Steinmetz and Brow, 1996)
YM838	LS20 *arp5*Δ*::KANMX*	This study
YM850	BY4741 *PCF11-3XHA::HIS3*	This study

YM885	LS20 *RPB1-3XFLAG::KANMX*	This study
YM900	BY4741 *PCF11-3XHA::HIS3 INO80-5XFLAG::NATMX*	This study
YM901	BY4741 *NRD1-3XHA::HIS3 INO80-5XFLAG::NATMX*	This study
YM903	LS20 *RPB1-3XFLAG::KANMX ino80Δ::HPHMX*	This study
YM1002	46a *arp8Δ::HPHMX*	This study
YM1036	46a *nrd1-5 arp8Δ::HPHMX*	This study
YM1085	LS20 *xrn1Δ::KANMX*	This study
YM1139	LS20 *rrp6Δ::KANMX*	This study
YM1141	46a *rco1Δ::KANMX*	This study
YM1147	46a *nrd1-5 arp8Δ::HPHMX rco1Δ::KANMX*	This study
YM1161	LS20 *rrp6Δ::KANMX arp8Δ::HPHMX*	This study
YM1325	LS20 *NAB2-3XHA::KANMX*	This study
YM1331	LS20 *NAB2-3XHA::KANMX ino80Δ::HPHMX*	This study
YM1332	LS20 *NAB2-3XHA::KANMX ino80Δ::HPHMX*	This study
YM1452	LS20 *NAB2-3XHA::KANMX htz1Δ::HPHMX*	This study

Supplementary Table 2 – Expression of genes encoding for RNA surveillance proteins is similar in WT, *ino80Δ* and *arp8Δ* cells. RNA abundance for the listed genes was measured by spiked-in total RNA-seq analysis in the indicated strains. Values represent average from two biological replicates for each experiment. The RNA-seq experiment for WT(1) and *ino80Δ* was conducted independently from WT(2) and arp8*Δ*. Values represent average from two biological replicates for each experiment.

Pathway/complex	Gene	WT(1)	*ino80Δ*	Fold Change	WT(2)	*arp8Δ*	Fold Change
NNS	*NRD1*	0.61	0.67	**1.1**	0.43	0.37	**0.8**
	NAB3	0.54	0.44	**0.8**	0.30	0.30	**1.0**
	SEN1	0.46	0.58	**1.3**	0.29	0.25	**0.8**
Exosome	*RRP6*	0.68	0.54	**0.8**	0.46	0.46	**1.0**
	DIS3/RRP44	0.82	0.73	**0.9**	0.64	0.62	**1.0**
TRAMP	*MTR4*	0.97	0.74	**0.8**	0.87	0.89	**1.0**
	TRF4	0.45	0.48	**1.1**	0.28	0.32	**1.1**
	AIR1	0.38	0.30	**0.8**	0.29	0.29	**1.0**
	AIR2	0.21	0.22	**1.1**	0.11	0.15	**1.4**
Cleavage and Polyadenylation	*HRP1*	1.21	1.01	**0.8**	1.04	0.83	**0.8**
	PCF11	0.26	0.24	**0.9**	0.19	0.18	**1.0**
	NAB2	0.70	0.59	**0.8**	0.51	0.54	**1.1**
	PAB1	8.95	6.85	**0.8**	4.53	3.89	**0.9**
Capping	*CEG1*	0.42	0.44	**1.1**	0.19	0.22	**1.1**
	CET1	0.27	0.26	**1.0**	0.17	0.19	**1.1**
Early mRNA processing	*CBC1*	0.96	0.74	**0.8**	0.58	0.68	**1.2**
	GBP2	1.43	1.09	**0.8**	0.83	0.74	**0.9**
	THO2	0.48	0.51	**1.0**	0.27	0.31	**1.2**
Export	*MEX67*	0.52	0.50	**1.0**	0.32	0.34	**1.1**
Cytoplasmic decay	*XRN1*	1.87	1.76	**0.9**	0.91	0.91	**1.0**
	SKI2	0.40	0.40	**1.0**	0.28	0.31	**1.1**

Supplementary Table 3 – Readthrough index (RI) of budding yeast *SNR* snoRNA genes as measured by total RNA-seq from the indicated strains. The RNA-seq experiment for WT(1) and *ino80Δ* was conducted independently from WT(2), *xrn1Δ*, *rrp6Δ*. Values represent average from two biological replicates for each experiment.

	WT(1)	***ino80Δ***	**WT(2)**	***xrn1Δ***	***rrp6Δ***
NME1	0.05	0.10	0.09	0.12	0.06
SNR11	0.18	0.17	0.26	0.23	0.24
SNR128	0.29	0.36	0.36	0.38	0.29
SNR13	0.15	0.28	0.44	0.36	0.25
SNR161	0.20	0.21	0.30	0.20	0.15
SNR189	0.22	0.23	0.47	0.39	0.33
SNR190	0.01	0.01	0.01	0.01	0.01
SNR3	0.90	1.05	0.91	0.87	0.68
SNR30	0.11	0.16	0.25	0.24	0.51
SNR31	0.18	0.15	0.17	0.17	0.13
SNR32	0.64	0.63	0.73	0.83	0.67
SNR33	0.41	0.39	0.47	0.37	0.51
SNR34	0.49	0.55	0.55	0.41	0.29
SNR35	0.17	0.20	0.27	0.17	0.17
SNR36	0.36	0.38	0.33	0.29	0.25
SNR37	0.32	0.37	0.46	0.42	0.72
SNR39B	0.41	0.57	0.50	0.41	0.93
SNR4	0.17	0.18	0.18	0.15	0.34
SNR40	0.61	0.70	0.62	0.70	0.53
SNR41	0.23	0.22	0.22	0.31	0.34
SNR42	0.42	0.37	0.98	0.59	0.95
SNR43	0.23	0.24	0.35	0.40	0.73
SNR45	1.15	1.04	0.99	0.84	1.57
SNR46	0.37	0.58	0.52	1.06	0.20
SNR47	0.56	1.21	0.52	0.56	1.61
SNR48	0.59	0.71	0.75	0.76	0.93
SNR49	0.53	0.62	0.43	0.41	0.21
SNR5	0.42	0.44	0.53	0.45	0.57
SNR50	1.30	1.08	1.00	0.97	1.76
SNR51	0.79	1.30	1.03	0.76	1.45
SNR52	0.47	0.51	0.52	0.42	0.60
SNR53	0.54	0.79	0.52	0.65	0.74
SNR55	0.39	0.57	0.42	0.55	0.28
SNR56	0.40	0.68	0.46	0.52	2.72
SNR57	0.66	0.64	0.60	0.62	0.71
SNR58	1.01	0.87	1.14	0.69	1.07

SNR61	1.57	2.83	1.19	0.85	2.76
SNR62	1.78	2.03	1.66	1.51	3.55
SNR63	0.40	0.52	0.66	0.43	0.55
SNR64	0.33	0.49	0.22	0.23	0.49
SNR65	0.74	0.95	1.09	0.30	3.17
SNR66	1.23	2.42	1.07	1.33	1.74
SNR67	1.07	1.01	1.08	1.14	1.44
SNR68	0.36	0.75	0.82	0.60	1.09
SNR69	0.68	0.88	0.75	0.80	0.70
SNR70	1.56	1.72	2.16	2.34	1.28
SNR71	1.38	2.61	1.41	1.39	3.46
SNR72	0.39	0.62	0.33	0.37	0.42
SNR74	1.10	1.29	1.05	1.53	0.47
SNR75	2.10	2.46	1.72	2.14	1.37
SNR76	0.57	0.52	0.46	0.44	0.30
SNR77	1.07	1.27	1.07	1.13	0.62
SNR78	3.67	4.40	4.26	5.35	4.26
SNR79	1.73	1.63	1.65	1.23	2.45
SNR8	0.27	0.27	0.21	0.22	0.27
SNR80	0.06	0.17	0.14	0.13	0.23
SNR81	0.15	0.28	0.23	0.19	0.12
SNR82	0.66	0.77	0.92	0.89	0.94
SNR83	0.35	0.46	0.46	0.30	1.03
SNR84	0.58	0.77	0.60	0.81	0.26
SNR85	0.02	0.02	0.03	0.02	0.08
SNR86	0.41	0.40	0.25	0.26	0.17
SNR87	0.93	1.16	1.04	0.90	1.38
SNR9	0.28	0.32	0.38	0.36	0.27

METHODS

Total RNA-seq assay.

Yeast strains were processed in duplicate. ERCC RNA Spike-in control mixes (Ambion, catalogue #4456740) were added to 1µg of total RNA according to manufacturer. Ribosomal RNAs were depleted from total RNA using the RiboMinus™ Eukaryote v2 Kit (Life Technologies). Depletion efficiency and quality control of rRNA-depleted RNA was assessed by analysis in RNA Pico 6000 chip for 2100 Bioanalyzer (Agilent). Total RNA-seq libraries were prepared from 50ng of rRNA-depleted RNA using the TruSeq® Stranded Total RNA Sample Preparation Kit (Illumina). Paired-end sequencing (2x50 nt) was performed on a HiSeq 2500 sequencer giving between 65 and 84 million reads. Reads were mapped using version 2.0.6 of TopHat, with a tolerance of 3 mismatches and a maximum size for introns 2Kb. Tags densities were normalized on spike-in controls for all subsequent analyses.

NET-seq assay.

NET-seq was performed from yeast strains containing Rpb1-FLAG (3XFLAG), alone or along with deletion of *INO80*. All strains appeared fully functional, with identical Ser2 and Ser5 phosphorylation levels on Rpb1 C-terminal domain and identical growth rates to the respective untagged strains (data not shown). NET-Seq libraries were constructed from biological duplicates of YM903 (*ino80Δ*, *RPB1-FLAG*) and YM885 (WT, *RPB1-FLAG*) cells and sequenced as previously described in (Wery et al., 2018). After removal of the 5'-adapter sequence, reads were uniquely mapped to the reference genome (ASM294v2.30) using version 0.12.8 of Bowtie (Langmead et al., 2009), with a tolerance of 2 mismatches. Data were normalized on the total number of uniquely mapped reads for each sample, as is commonly done in the majority of NET-seq studies in yeast, in accordance with standard procedures (Churchman and Weissman, 2012).

ChIP-exo assay.

The ChIP-exo assay has been previously described (Rhee and Pugh, 2012). In brief, yeast strains were grown to exponential phase in yeast extract peptone (YP) + 2% dextrose (30°C to OD600 nm = 0.8), then subjected to 1% formaldehyde crosslinking for 15 min at 25 °C. After quenched with 125mM final concentration of glycine for 5 min, cells were harvested and washed. Sonicated chromatin was prepared by standard methods. Standard ChIP methods were used for histone H3 (antibody Ab1791, Abcam) followed by lambda exonuclease treatment and library construction. Libraries were sequenced on an Illumina 2000 sequencer. Reads were uniquely mapped to the reference genome (sacCer3 build) using version 2.1.0 of Bowtie2 (Langmead and Salzberg, 2012) with a tolerance of 1 mismatch in seed alignment. Data were normalized on the total number of uniquely mapped reads, for each sample.

Cell proliferation analysis in liquid media assay.

Liquid growth rate analysis was conducted using the CG-12 robot (S&P Robotics Inc.). Yeast cells transformed with a *URA3*-containing plasmid (pRS416) and grown exponentially in SC-ura at 30°C were diluted to OD^{620} 0.1 in either SC-ura or SC-ura + 50µg/ml 6-AU and four 150µl samples from each strain were plated onto 96-well transparent plates covered with breathable films. Plates were incubated at 30°C for several days and OD^{620} was measured in the CG-12 robot (S&P Robotics Inc.) every hour with a shaking of 1000rpm for 1 minute before each read. Liquid growth rate analysis was not possible in the *nrd1-5* derived strains due to flocculation. All cell proliferation experiments were repeated at least twice.

Growth rates analysis on agar plates assay.

Growth of yeast strains was compared by plating 5-fold serial dilutions on SC / SC-inositol, SC-ura / SC-ura + 50µg/ml 6-azauracil (6-AU, Sigma), SC-leu / SC-leu + 0.4mM $CuSO_4$ (Sigma) or SC-leu / SC-leu + 0.25 $CuSO_4$ and incubating the plates at 30°C for several days. All plating experiments were performed at least three times.

RT-qPCR assay.

Total RNA was extracted either with RNeasy Mini Kit (Qiagen) or by classical acid phenol-chloroform extraction. RNAs abundance was measured with SuperScript® III Platinum® SYBR® Green One-Step qRT-PCR Kit (Invitrogen) using specific primers for the targets of interest in a 10µl reaction volume, on Applied Biosystem Step-One Plus machines. RNAs abundance of each sample was compared with standard curves analysis. Abundance of *CUP1* from transcriptional read-through analyses using the *ACT-CUP* reporter system was compared to *ACT** RNA specifically transcribed from the same plasmid (Figure S4C). Abundance of *NRD1* promoter-proximal RNA (*NRD1* 5') was compared to levels of *NRD1* promoter-distal RNA (*NRD1 3'*).

Co-immunoprecipitation assay.

Benzonase-treated yeast cell extracts were incubated with 20µl Anti-FLAG Affinity Gel (Sigma Aldrich) in 10mM Tris-Cl pH 7.5, 150mM NaCl, 0.05mM EDTA, 0.5% NP40, 1X Protease Inhibitor Cocktail (Roche) and 0.01mM PMSF for 3h. Beads were washed twice in 10mM Tris-Cl pH 7.5, 150mM NaCl, 0.05mM EDTA, 1X Protease Inhibitor Cocktail (Roche) and 0.01mM PMSF and resuspended in SDS sample buffer. Western blot analyses were performed using Monoclonal anti-FLAG M2 antibody (Sigma F3165), Anti-HA tag antibody (Abcam, ab9110) and Anti-Arp5 antibody (Abcam, 12099). Images were acquired using Syngene G:BOX. The experiment was reproduced three times.

Immunoprecipitations for H2A.Z and HA-tag were performed similarly on benzonase-treated yeast cell extract using 36µl Protein-A sepharose beads coupled with 6µl of appropriate antibody (Anti-H2A.Z, Active Motif 39647; Anti-HA tag, Abcam ab9110). Control immunoprecipitations (mock) were performed with a specific antibody (Anti-Rabbit IgG, Promega). Western blot analyses were performed using the following antibodies: Anti-HA, Anti-Arp5, Anti-H2A.Z and Anti-Rpb1 y-80 (Santa Cruz Biotechnology, sc-25758). After the immunoprecipitation for H2A.Z shown in Figure S6G, beads were washed twice in 10mM Tris-

Cl pH 7.5, 150mM NaCl, 0.05mM EDTA, 1X Protease Inhibitor Cocktail (Roche) and 0.01mM PMSF, then washed a third time in the same buffer containing 300mM NaCl and finally resuspended in SDS sample buffer All experiments were reproduced three times.

Ino80 inducible degradation assay.

The assay for inducible degradation of Ino80 (Jonsson et al., 2004) was performed as previously described (Lafon et al., 2015a; Papamichos-Chronakis and Peterson, 2008). Briefly, a degron tag was fused to *INO80* (*Ino80-td*) in cells carrying the *UBR1* gene, that encodes for the N-recognin Ubr1, under the control of the *GAL1* promoter, and cells were transformed with the *ACT-CUP* plasmid reporter system (Figure S4C). Cells were grown in SC-leu media containing raffinose as carbon source at 25°C until OD^{600}~0.6-0.7, then shifted to SC-leu media containing galactose to induce *UBR1* expression. Subsequently, complete *Ino80-td* protein degradation by the Ubr1 pathway was induced by 3 hours of heat shock at 37°C. Cells were then immediately harvested by centrifugation at 4°C, 3500rpm for 3 minutes, then washed twice with ice-cold water and snap-frozen in liquid nitrogen for RNA analysis. Yeast cells carrying the *GAL1*-driven *UBR1* gene along with an unmodified *INO80* genes were use as control. Furthermore, both (*GAL1-UBR1*) and (*GAL1-UBR1 Ino80-td*) cells were grown in SC-leu media containing glucose as a negative control for *UBR1* expression (Figure 4H and Figure S4F, grey bars). RNA analysis was conducted by RT-qPCR as described above.

ChIP-qPCR assay.

Chromatin immunoprecipitation was performed as previously described in (Papamichos-Chronakis et al., 2011). Sonication was performed on a Bioruptor® Pico sonication device (Diagenode) with ten 30-sec pulses with a 30-sec break between pulses. Immunoprecipitation was carried out with Anti-HA tag antibody (Abcam ab9110) and Anti-Rpb1 y-80 antibody (Santa Cruz Biotechnology, sc-25758) in parallel. The recovered DNA was subjected to quantitative real-time PCR using Platinum® SYBR® Green qPCR SuperMix-UDG Kit

(Invitrogen) with specific primers for the targets of interest in 10µl reaction volume, on Applied Biosystem Step-One Plus machines.

RNA-IP assay.

RNA immunoprecipitation was performed as described in (Selth et al., 2009). Sonication was performed on a Bioruptor® Plus sonication device (Diagenode) with two 15-sec pulses at 50% amplitude with a 1-min break between pulses. Immunoprecipitation was carried out with Anti-HA tag antibody (Abcam ab9110). The recovered RNA was analysed by RT-qPCR as described above.